Supporting Information

Self-powered NH_3 synthesis by trifunctional Co_2B based high power density Zn-air batteries

Divyani Gupta,[a] Alankar Kafle,[a] Prajna Parimita Mohanty,[b,c] Tisita Das,[c] Sudip Chakraborty,[c] Rajeev Ahuja,[b,d] Tharamani C. Nagaiah[a]*

[a]*Department of Chemistry,* [b]*Department of Physics, Indian Institute of Technology Ropar, Rupnagar, Punjab-140001, India*

[c]*Materials Theory for Energy Scavenging (MATES) Lab, Harish-Chandra Research Institute(HRI)Allahabad, HBNI, Chhatnag Road, Jhunsi, Prayagraj (Allahabad) 211019 India*

[d]*Condensed Matter Theory Group, Department of Physics and Astronomy, Uppsala University, Uppsala, SE-75120, Sweden*

Materials used

All the chemicals and reagents used in this study are of analytical grade and used without further purification. Cobaltous chloride ($CoCl_2.6H_2O$, 99%, extra pure) was purchased from SDFCL and sodium borohydride ($NaBH_4$, anhydrous) was purchased from Sigma-Aldrich. Hydrochloric acid (HCl, 37%) was bought from Merck. Other chemicals including ammonium chloride (NH_4Cl, 99%), salicylic acid ($C_7H_6O_3$, 99.5%), sodium nitroprusside ($C_5FeN_6Na_2O$, 99%), para-dimethylaminobenzaldehyde (p-$C_9H_{11}NO$, 99%), sodium nitrate ($NaNO_3$, 99%), sodium nitrite ($NaNO_2$, 98%), sulphanilamide ($C_6H_8N_2O_2S$, 99%), N-(1-Napthyl) ethylenediamine dihydrocholoride ($C_{12}H_{14}N_2$, 99%), trisodium citrate ($Na_3C_6H_5O_7$) were bought from Loba Chemie. Reagents including sodium sulphate (Na_2SO_4, 99%) and potassium hydroxide (KOH, 85%), sodium hydroxide (NaOH, 98%), hydrazine monohydrate (N_2H_4.H2O, 99%), sodium hypochlorite solution (NaClO, 4-6%) and hydrogen peroxide solution (H_2O_2, 5%) were also purchased from Loba Chemie. High purity $^{14}N_2$ (99.999%), $^{15}N_2$ (99%) and Ar gas (99.999%) cylinders were purchased from Sigma. All solutions were prepared using deionized water obtained from Millipore system (>15 MΩ).

Experimental Section

Catalyst synthesis

The Co_2B (1:8) catalyst was synthesized thru environment friendly sonochemical technique using non-expensive precursors. Briefly, 1 mmol of $CoCl_2.6H_2O$ (476 mg) was added in a round bottom flask (RBF) and dissolved in 40 mL of deionized water (Solution A). The solution in RBF was kept under inert atmosphere and ultrasonication for 10 minutes using a bath sonicator filled with ice cold water. Further, 8 mmol of $NaBH_4$ solution (302 mg in 10 mL deionized

water) *i.e.* solution B as reducing agent, was added dropwise into solution A under continuous bath sonication and probe sonication at regular intervals (15 second sonication and 30 second rest) using ultrasonic horn at a frequency of 20 Hz subsequently. After the complete addition of solution B into solution A, the reaction mixture was kept undisturbed for reaction completion (confirmed from disappearance of bubble evolution).
Reactions taking place during the synthesis are mentioned as follows:

$$2CoCl_2\,(aq.) + 2NaBH_4(aq.) + 9H_2O \longrightarrow Co_2B\,(s) + 4\,NaCl\,(aq.) + 12.5\,H_2(g) + 3\,B(OH)_3(aq.)$$

In the end, the precipitates formed were collected via centrifugation and washed 3-4 times by mixture of ethanol: water (1:1, v/v) and kept for drying overnight at 60 °C under vacuum to obtain precipitates, denoted as Co_2B (Metal : Boron). The Metal: Boron ratio was varied as 1:4/1:8/1:12 mmol in this study.

Electrochemical analysis for NRR/ORR/OER

All the electrochemical experiments for ORR and OER were performed in a single compartment electrochemical cell. The electrochemical studies for NRR were performed at room temperature in a home made two compartment H-cell, separated by a Nafion N117 membrane. Before fitting the membrane, it was boiled in deionized water (>15 MΩ) for 30 min., followed by heat treatment at 80 °C in H_2O_2 (5%) solution for another 30 min., after which it was finally boiled in 0.05 M H_2SO_4 for 1 h. The experiments were performed with three electrode assembly consisting of working electrode (WE), a home-made double junction Ag/AgCl/3M KCl as reference electrode (RE) and Pt wire as counter electrode (CE) in 0.1 M KOH electrolyte solution. A Teflon-embedded glassy carbon (GCE Ø 5mm, Pine instrument, USA) disk electrode with Pt ring was used as a working electrode for RRDE analysis and glassy carbon (Ø 2mm) electrode was utilised for the rest of the electrochemical analysis *viz.,* CV, EIS, ECSA, etc. Catalyst was physically grinded in mortar pestle for 30 min. to obtain fine powder. To prepare the catalyst ink, catalyst powder was taken (all the variants; 1.5 mg) and dispersed in the mixture of isopropyl alcohol (20 µL) and deionized water (480 µL) and further ultrasonicated to get homogeneously dispersed catalyst ink. Afterwards, the ink was drop-casted on GC electrode surface and dried at room temperature under atmospheric conditions. Before coating the catalyst ink onto the GCE, it was polished on a Nylon polishing cloth (SM 407052, AKPOLISH) using alumina paste of different grades (0.5, 0.3, 0.05 µm; Pine instrument, USA) to acquire mirror finishing followed by thorough washing and ultrasonication in deionized water to remove any physisorbed alumina particles over its surface. RRDE experiments were performed using Autolab 302N modular potentiostat/galvanostat analysed by NOVA 1.11 software. The hydrodynamic experiments were carried out at different rotation rates using a speed controlling unit (AFMSRC, Pine research instrument Inc., USA). Other measurements including linear sweep voltammetry

(LSV), chronoamperometry, electrochemical impedance spectroscopy (EIS) and cyclic voltammetry (CV) were performed using Biologic VSP 300 Potentiostat.

Zn-air battery

A home-made battery cell was utilized to assess the performance of catalyst as an air cathode. Air cathode consist of catalyst layer (CL), nickel foam and gas diffusion layer (GDL) respectively. CL was fabricated using Co_2B as catalyst in N-Methyl-2-pyrrolidone (NMP) solvent. Mixture of polyvinyldene fluoride (PVDF) and vulcan carbon (VC) (1:1, ratio by weight) was dispersed in NMP after grinding to a fine powder using ultrasonication for 30 min. in bath sonicator and slurry was coated onto the Ni foam substrate as GDL. On other side of Ni foam substrate, catalyst layer was coated followed by drying and pressing under the pressure of 2.5 MPa. Finally, Zn-air battery was assembled with polished Zn foil (99.5%, extra pure) as the anode, 6 M KOH and 0.2 M $Zn(ac)_2$ as the electrolyte and prepared air cathode (geometric area of 0.1256 cm^2, catalyst loading of 2 mg cm^{-2}) in home-made cell setup. For a better comparison, Zn-air battery was assembled using mixture of commercial Pt/C (20%) and RuO_2 (1:1 ratio by weight) as catalyst layer. All measurements were carried out under ambient conditions of temperature and pressure using Biologic VSP-300 potentiostat. Linear sweep voltammetry was employed to obtain the polarization curves at a scan rate of 5 mV s^{-1}. The galvanostatic charge-discharge cycling (10 min. discharge and 10 min. charge at ± 10 mA cm^{-2} respectively) were performed for 25 h. Both the current density and power density were normalized to the effective surface area of air cathode.

Battery powered NH_3 production

The rechargeable Zn-air battery equipped with Co_2B (1:8) as air cathode was used to conduct NRR measurements. We have built a homemade two-electrode NRR setup wherein two batteries connected in series (2.9 V) were used as the power supply and a 300 Ω resistor was used as voltage divider. Quantification of ammonia produced during electrolysis was measured using similar set of experiments previously in experimental section.

Physical characterization

The P-XRD patterns for catalysts were investigated with PANalytical X'PERT pro diffractometer in the 2θ range of 5-80° using Cu-Kα radiation (λ=0.1542 nm, 40kV, 40mA) with a scan speed of 2° per minute and a proportional counter detector to acquire structural information. The morphological analysis was done using field emission-scanning electron microscopy (FE-SEM, Hitachi, Japan, SU8010) and transmission electron microscopy (HR-TEM, JEOL, Jem 2100 plus). The high resolution TEM (HR-TEM) images were recorded at 200 kV. To attain the electronic attributes of catalyst, XPS measurements were performed with the Thermo scientific NEXSA surface analysis with a micro-focused (400 µm, 72 W, 12000 V) monochromatic Al Kα (1486.6 eV) a hemispherical analyser and 128 channel plate detectors under ultrahigh vacuum (UHV 8-10 mbar). The obtained spectra were calibrated with C 1s spectra. Quantification of various impurities and products formed during NRR were tested using an (SEC2000-DH) UV-vis

Spectrometer. Water contact angle (WCA) measurements measured were performed using a First Ten Angstroms (FTA) Contact Angle System by sessile water drop method under room temperature conditions by using water as a probe liquid with a volume of 0.6 µL in a needle with width of 0.305 mm. The average WCA (θ H_2O) was then determined for the different samples. The surface hydrophobicity properties of all catalyst variants ware studied by WCA measurements. Homogeneous suspension of catalyst (1 mg) mixed with water (20 µL) was drop-casted onto the Teflon tape rolled over glass slide followed by drying at room temperature. After which the water drops were deposited with the help of sessile water syringe.

Quantification of products/contaminants

Quantification of NH_3 by Indophenol blue method[1]

The final product (*i.e.* NH_3) obtained after electrolysis was quantified using indophenol blue method with the help of SEC2000 spectrometer system. Firstly, 2 mL of electrolyte sample (after 2 h chronoamperometry) was collected from the cathodic compartment of H-cell in which 2 mL of solution containing mixture of 5% salicylic acid and 5% trisodium citrate in 1 M KOH was added immediately. Consequently, 1 mL of 0.05 M NaClO and 200 µL of 1% sodium nitroprusside as a colouring agent was added thereafter to the same electrolyte sample. The solution was incubated for 2 h to develop stable colour, and absorbance was measured at a wavelength of 655 nm using UV-vis spectroscopy. Initially, the UV-vis spectrum were obtained for different concentrations of NH_3 (0.2, 0.4, 0.8, and 1 ppm) using standard NH_4Cl solution, which was further utilised to obtain a calibration curve exhibiting a linear relationship between absorbance and concentration value from the fitting curve ($y = 0.285 x + 0.109$, $R^2 = 0.99663$). Afterwards, the amount of NH_3 in electrolyte samples collected after NRR was quantified using standard calibration curve.

Quantification of N_2H_4 by Watt-Chrisp method[1]

Presence of N_2H_4 in the electrolyte sample after NRR was confirmed using Watt and Chrisp method. Briefly, 0.3 g of p-$C_9H_{11}NO$ was mixed with 2 mL of HCl and 20 mL of ethanol to obtain the final colouring solution. A series of standard solutions of N_2H_4 (0.1, 0.2, 0.4, 0.8, and 1 ppm) were prepared and 2 mL of which was separately mixed with 2 mL of above prepared colouring solution. Afterwards, the solution was kept under incubation for 20 min. at R.T. to achieve stable color and measure absorbance at 455 nm using UV-vis spectrometer. The as-obtained calibration curve ($y = 0.285 x + 0.109$, $R^2 = 0.99663$), exhibit a good linear relationship between absorbance and N_2H_4 concentrations respectively. The determination of amount of hydrazine formed in electrolyte sample after NRR was estimated similarly using the standard calibration curve.

Quantification of NH_3 by Nessler's reagent method [2]

The quantified NH_3 yield was validated by other quantification method *i.e.* Nessler's reagent test. The preparation of Nessler's reagent was initiated by the addition of 2.5 g of mercuric iodide into 5 mL aq. solution of potassium iodide (2 g in 5 mL deionized water) followed by its dilution upto 20 mL using deionized water. To the above solution, 4 g of NaOH was added thereafter, denoted herein as Nessler's reagent. For quantification of produced ammonia, 5 mL of electrolyte solution obtained after electrolysis was collected to which 0.25 mL of sodium potassium tartrate (500 g L^{-1}) and 0.25 mL of Nessler's reagent was added. The above solution mixture was kept undisturbed for 10 minutes and then measurement was performed using UV-Vis. spectrophotometer at a wavelength (λ) of 420 nm. The calibration curve was extracted from the different standard NH_4Cl solutions with known NH_4^+ concentrations in the range of 0.1, 0.2, 0.4, 0.8, and 1.0 µg mL^{-1} in a similar way.

Isotope labelling experiments [3]

The isotope labelling experiment was performed by taking $^{15}N_2$ (Sigma-Aldrich 99 atom% ^{15}N) as the feeding gas during NRR for possible $^{15}NH_4^+$ production. A fixed amount of gas (200 mL) was supplied to the NRR cell during the electrolysis for 2 h. After electrolysis 25 ml of the electrolyte was taken out and mixed with 1M HCl and then concentrated to 1 mL, from which 0.6 ml of the resulting liquid was taken and 0.4 ml of DMSO-d_6 was added as an internal standard. The produced ammonia was confirmed by using ^1H nuclear magnetic resonance measurements (^1H NMR) with water gate suppression sequence with a relaxation delay of 3 s, 8000 scans using a pulse sequence by pulse field gradient (PFG) unit. All other samples ($^{14}N_2$ and Ar saturated) were tested in the similar manner.

Purification of gas-supplies

Prior to each NRR measurement, the $^{15}N_2$ gas was passed through alkaline $KMnO_4$ followed by dilute H_2SO_4 solution (scrubbing solution) to remove any trace NH_4^+ and NO_X (NO, NO_2, N_2O) impurities. The impurities were quantified using colorimetric method and gas chromatography-mass spectroscopy (GC-MS) method by following the reported procedures. The NO_x (NO/NO_2) was trapped in alkaline $KMnO_4$ solution technique while NH_4^+ impurities were trapped in acidic solution and both were quantified using UV-Vis. spectrophotometry before and after purification. On the other hand, the N_2O impurities were detected and quantified by means of GC-MS in SIM (selected ion monitoring) mode at m/z value of 44 for N_2O. For N_2O detection in GC-MS via SIM acquisition mode, the column oven temperature was set at 40 °C with an injection temperature of 150 °C, column flow of 0.99 mL min^{-1}, ion source temperature of 200 °C, interface temperature of 220 °C.

Detection of NO_2^- and NO_3^- contaminants in electrolyte[4]

Amount of NO_3^- present in the electrolyte i.e. 0.1 M KOH was determined using UV-Vis. spectrophotometry, wherein the peak at 220 nm of wavelength corresponds to absorption of nitrates and the corresponding amount can be quantified with respect to measured absorbance value. Standard stock solutions with varying concentrations i.e. 0.2 ppm to 5 ppm

were prepared using $NaNO_3$ stock solution. Afterwards, 5 mL of standard along with sample solution were taken in glass vial to which 0.1 mL of 1 M HCl was added subsequently with frequent shaking. The solution was allowed to stand undisturbed for 5 min. and UV-vis. measurement was carried out in the range of 200-300 nm to obtain the analogous calibration curve.

On the other hand, diazotization reaction can be carried out for quantification of nitrites using sulphanilamide under acidic environment followed by coupling with N-(1-Napthyl) ethylenediamine dihydrocholoride, resulting into pink azo dyes exhibiting peak at 540 nm respectively. For quantification of NO_2^-, standard solutions were prepared using $NaNO_2$ stock solution with different concentrations *i.e.* 2 to 60 µg L^{-1}. Two reagents were prepared separately; 0.5 g of sulphanilamide in 50 mL of 2 M HCl *i.e.* **A** and 20 mg of N-(1-Napthyl) ethylenediamine dihydrocholoride in 20 mL of deionized H_2O *i.e.* **B**. At first, 5 mL of standard or sample solutions were taken in glass vials, to which 0.1 mL of A was added and allowed to stand for 10 min, followed by addition of 0.1 mL of B respectively. After mild shaking, the solution mixture was kept undisturbed for 30 min and amount of NO_2^- was estimated under wavelength range of 440-600 nm, from which calibration curves were extracted and plotted.

Electrochemical measurements

Electrochemical impedance spectroscopic (EIS) measurements

Calculation of charge transfer resistance was done to study the kinetics of the electrocatalysts at electrode/electrolyte interface by performing electrochemical impedance spectroscopy (EIS). A DC potential of -0.3 V *vs.* RHE (formal potential obtained after performing CV in N_2 saturated 0.1 M KOH) was applied over an AC perturbation of 10 mV between a frequency range of 100 Hz to 40 KHz in a logarithmic frequency step over a single sine wave. A typical semicircular behavior was observed in corresponding Nyquist plot from which solution resistance (R_s) was obtained at high-frequency region, polarization resistance (R_p) was obtained at low-frequency region, wherein the difference between the two gave charge transfer resistance (R_{ct}) respectively.

Pseudo-double layer capacitance calculation (C_{dl})

In order to determine the double layer capacitance of electrocatalysts, cyclic voltammetry was performed at different scan rates (10 mV s^{-1} to 320 mV s^{-1}) under the non-faradaic region between a potential window of 1 to 1.1 V *vs.* RHE in N_2 saturated 0.1 M KOH solution. The average current density obtained from CVs were plotted against scan rate, wherein, the value of slope provided the double-layer pseudo-capacitance. ECSA was further calculated by dividing C_{dl} by specific capacitance of flat standard surface *i.e.* taken as 40 µFcm^{-2} in this case.[5]

Calculations

The rate of ammonia formation was determined according to

$$Yield\ rate(\mu g\ cm^{-2}\ h^{-1}) = \frac{V \times C_{NH_3}}{t \times m_{cat.}}$$

Here, C_{NH3} is the measured NH_3 concentration, V the volume of electrolyte, *t* the time of the reduction reaction and m_{cat} is the mass of the catalyst loaded onto GCE. Similarly, its Faradaic efficiency (F.E.) was calculated as

$$F.E.\ (\%) = \frac{3 \times F \times V \times C_{NH3}}{17 \times Q}$$

Where F is the Faraday constant and Q is the total amount of charge passed through the electrodes during the electrolysis.
Calculations for specific capacity were done using the following equation:

$$Specific\ capacity\ = \frac{current\ \times discharge\ time}{weight\ of\ consumed\ zinc}$$

The energy density for the same were calculated according to following equation:

$$Energy\ density\ = \frac{current\ \times discharge\ time\ \times average\ discharge\ voltage}{weight\ of\ consumed\ zinc}$$

TOF_{NRR} calculations for Co_2B (1:8) catalyst;

$$Turnover\ frequency\ (TOF) = \frac{Turnover\ number\ (TON)}{Time\ (h)}$$

$$Turnover\ number\ (TON) = \frac{yield\ of\ NH_3\ obtained\ after\ NRR(mg)}{Loading\ of\ catalyst\ (mg)}$$

Where, time (t in hours) represents the total NRR electrolysis duration.

TON and TOF for the catalyst (Co_2B (1:8)) is calculated as follows:

$$TON = \frac{2.98022}{0.02983} = 1.49011;\ TOF = \frac{1.49011}{2} =\ 0.74\ h^{-1}$$

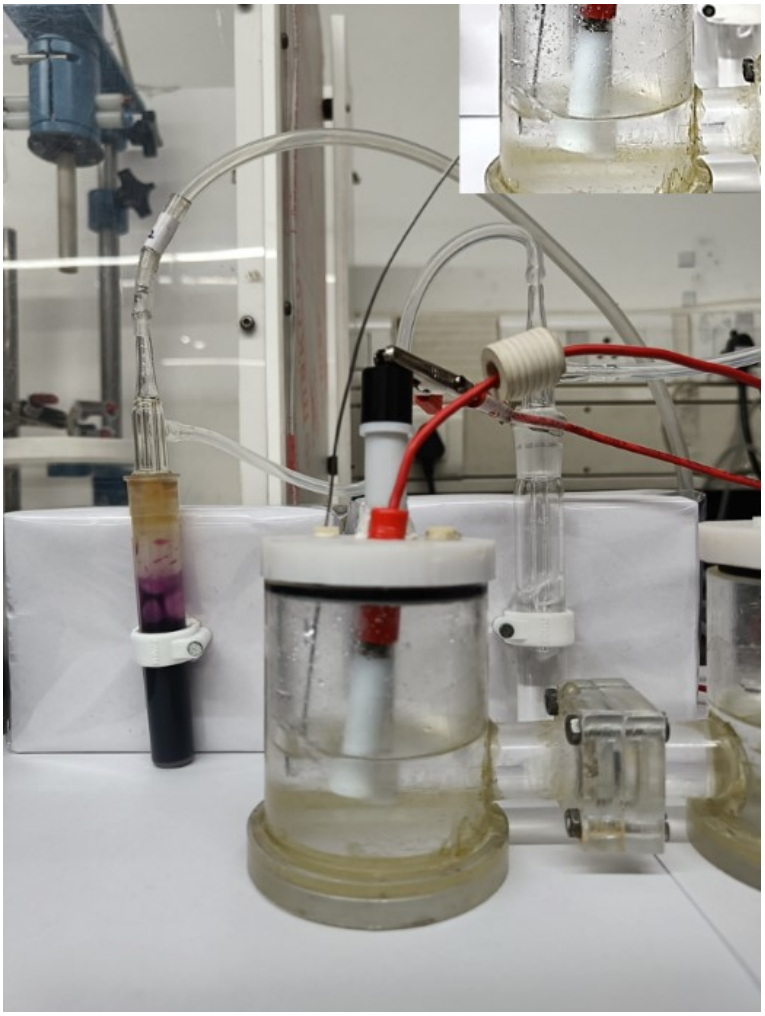

Fig. S1 Photograph of H-cell setup acquired for NRR with gas-streams passing through $KMnO_4$ and acid trap before starting the measurements.

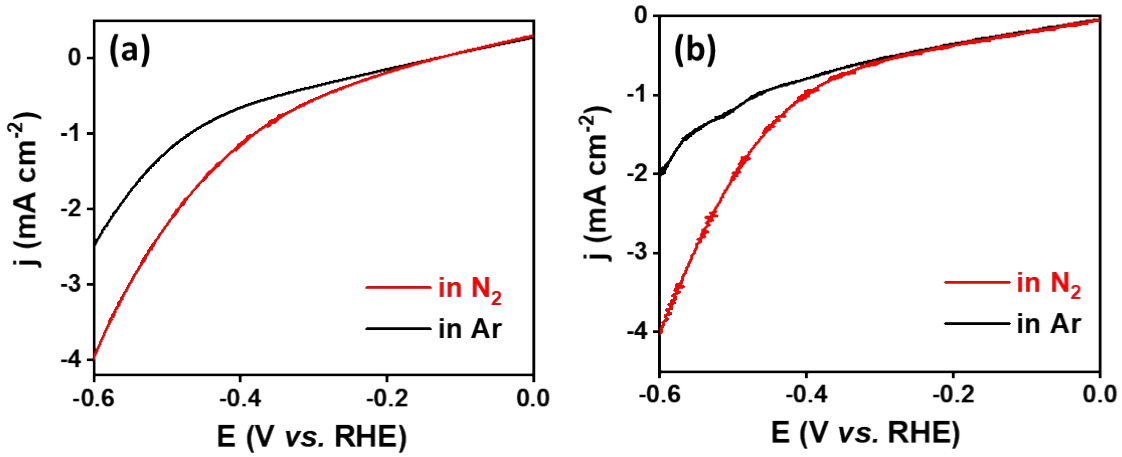

Fig. S2 Linear sweep voltammograms in Ar- and N_2- saturated 0.1 M KOH by (a) Co_2B (1:4) and (b) Co_2B (1:12) during NRR.

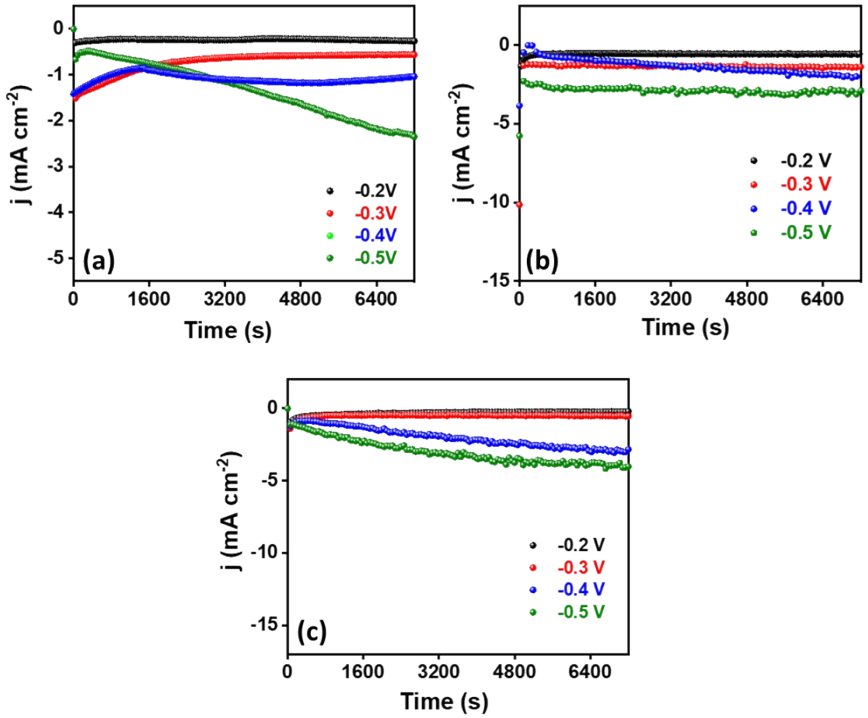

Fig. S3 Chronoamperometric curves recorded at different potentials for (a) Co_2B (1:4), (b) Co_2B (1:8) and (c) Co_2B (1:12) during NRR.

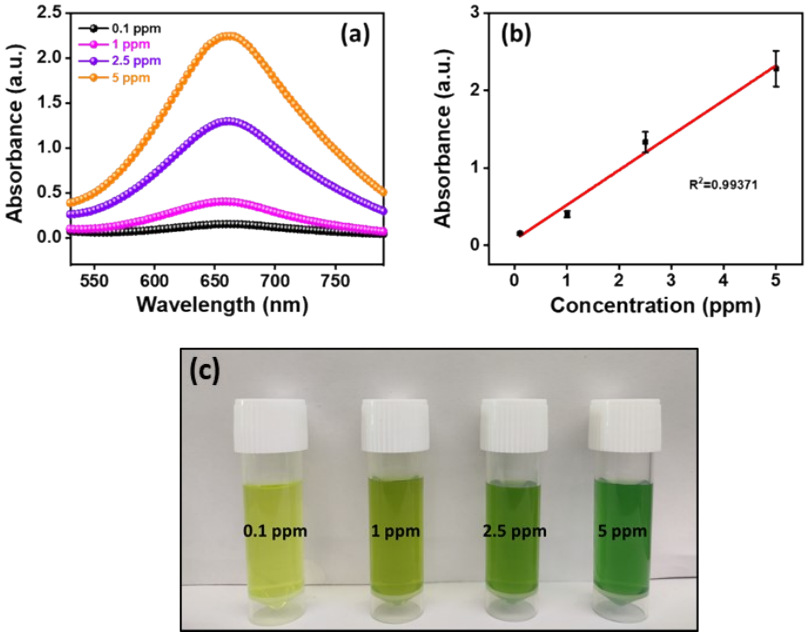

Fig. S4 (a) UV-Vis. Absorbencies for standard NH_3 solutions, (b) respective calibration curve by Indophenol blue method and (c) Photographs of standard NH_3 solutions with different concentrations captured during Indophenol blue method.

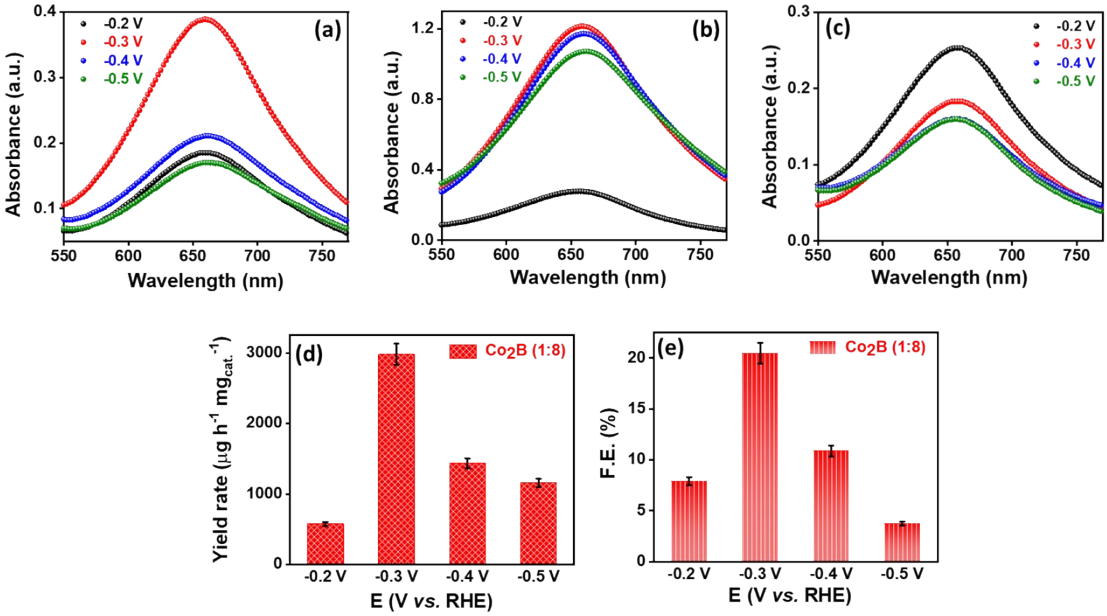

Fig. S5A UV-Vis. Absorbencies for (a) Co_2B (1:4), (b) Co_2B (1:8) and (c) Co_2B (1:12) after NRR at different potentials. (d) F.E. and (e) NH_3 production yield rates for Co_2B (1:8) at different applied potentials.

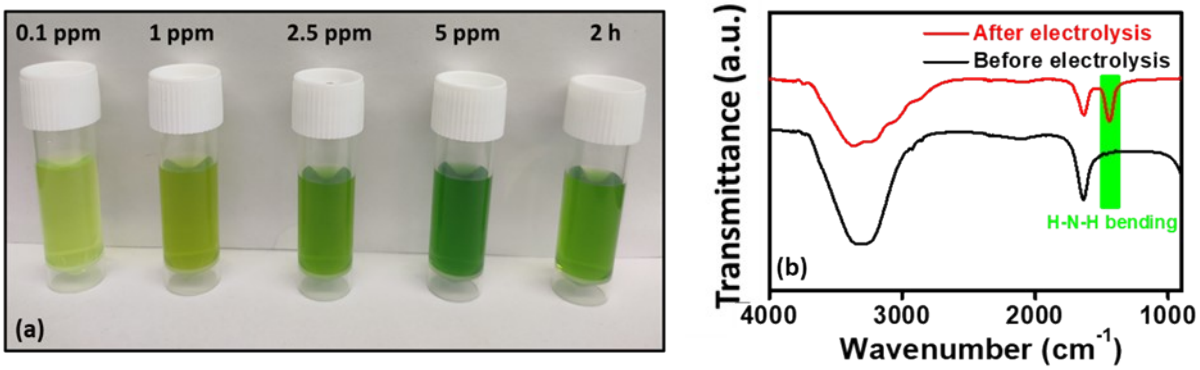

Fig. S5B (a) Image of electrolyte sample collected after 2h of chronoamperometry at -0.3 V (*vs.* RHE) by Co_2B (1:8) with standard NH_4^+ samples, (b) FT-IR spectra comparison of 0.1 M KOH and sample+0.1 M KOH solution obtained after NRR by Co_2B (1:8).

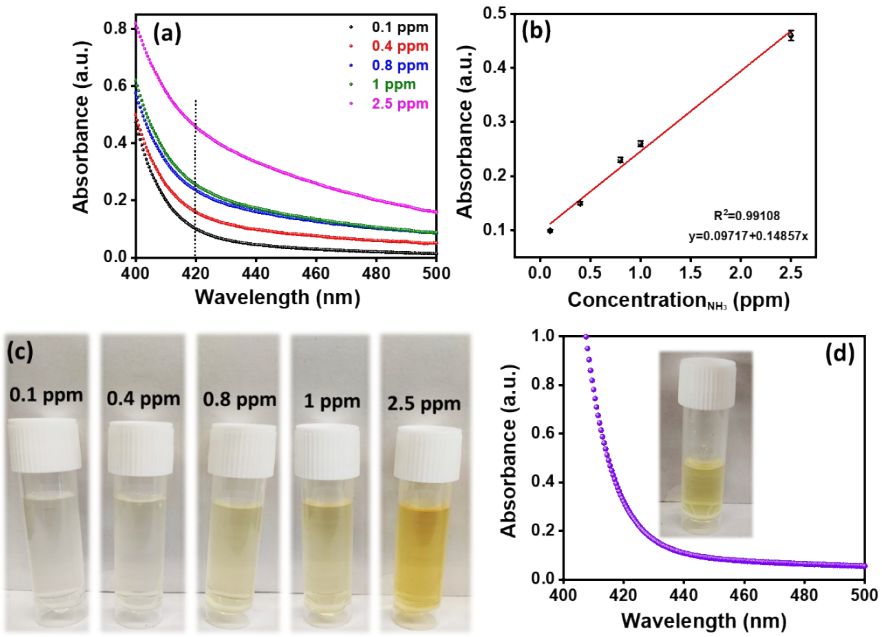

Fig. S5C UV-Vis. curves obtained for standard NH_4^+ solutions (different concentrations) after Nessler's reagent test and (b) corresponding calibration curve for quantification. (c) Photographs of color development of standard NH_4^+ solutions during Nessler's test. (d) UV Vis. absorbance curve for solution collected after 2 h electrolysis by Co_2B (1:8) in N_2-saturated 0.1 M KOH during Nessler's test.

Fig. S6 Quantification of N_2H_4 by Watt-Chrisp method by (a) standard N_2H_4 solutions at

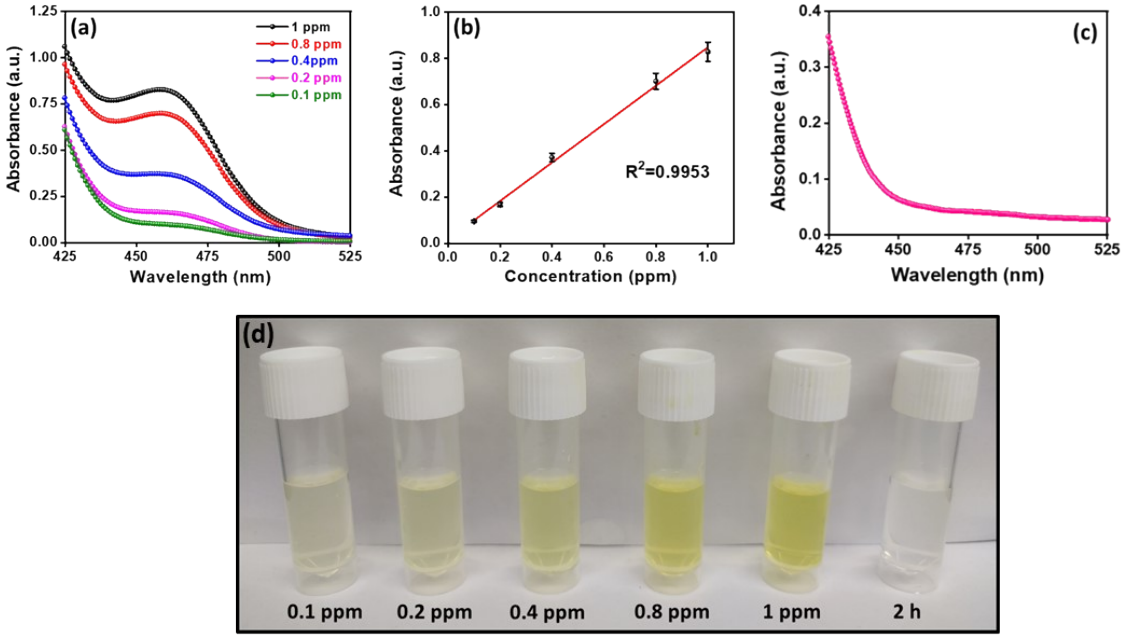

different concentrations and (b) respective calibration curve extracted from (a) and (d) Photographs of standard N_2H_4 solutions of different concentrations and electrolyte sample collected after NRR by Co_2B (1:8) at -0.3 V during quantification by Watt-Chrisp method.

Table S1A. Comparison of activity of recent reported catalysts towards NRR in alkaline media

Catalyst	Electrolyte	R_{NH3} (μg h^{-1} $mg_{cat.}^{-1}$)	Pot. *vs.* RHE	F.E. (%)	Ref.
MIL-100 (Al)/Cu	0.1 M KOH	10.6 μg h^{-1} cm^{-2} $mg_{cat.}^{-1}$	0 V	22.6	[6]
Co_3Fe–MOF	0.1 M KOH	8.79	-0.2 V	25.64	[7]
3D Rh particles	0.1 M KOH	35.58	−0.2 V	1.2 (0 V)	[8]
Cu SAC	0.1 M KOH	53.3	-0.35 V	13.8	[9]
Cu/PI-300	0.1 M KOH	12.4 μg h^{-1} cm^{-2}	-0.3 V	6.56	[10]
FeSA-N-C	0.1 M KOH	7.48 μg h^{-1} cm^{-2}	0 V	56.55	[11]
C-ZIF-1100-1 h	0.1 M KOH	9.22 mmol g^{-1} h^{-1}	-0.3 V	10.2	[12]
SA-Mo/NPC	0.1 M KOH	34.0 g h^{-1} mg_{cat}^{-1}	-0.45 V	14.6	[13]
PdRu TPs	0.1 M KOH	37.23	-0.2 V	1.85	[14]
Pd_3Cu_1	0.1 M KOH	39.9	-0.25 V	0.58	[15]
Rh NNs	0.1 M KOH	23.9	-0.2 V	0.217	[16]
Se-doped C	0.1 M KOH	1.14 μg h^{-1} cm^{-2}	-0.45V	3.92	[17]
Te-doped C	0.1 M KOH	1.91 μg h^{-1} cm^{-2}	-0.5 V	4.6	[17]
$FeWS_x$@$FeWO_4$-2	1 M KOH	16.6	-0.45 V	6.01	[18]
Ru@$Ti_3C_2T_x$	0.1 M KOH	2.3 μmol h^{-1} cm^{-2}	-0.4 V	13.13	[19]
Cu@$Ti_3C_2T_x$	0.1 M KOH	3.04 μmol h^{-1} cm^{-2}	-0.5 V	7.31	[20]
CuAg@$Ti_3C_2T_x$	0.1 M KOH	4.12 μmol cm^{-2} h^{-1}	-0.5 V	9.77	[21]
CoP hollow nanocage	1 M KOH	10.78	-0.4 V	7.36	[22]
Fe_3Mo_3C	1 M KOH	13.1 μg cm^{-2} h^{-1}	-0.5 V	0.26	[23]
Au/C	0.1 M KOH	9.39×10^{-11} mol cm^{-2} s^{-1}	-0.3 V	0.25	[24]
FL-Sb nanosheets	0.1 M KOH	133.1	0.05 V	11.6	[25]
CoPi/NPCS	0.1 M KOH	20.5	-0.2 V	7.07	[26]

CoPi/HSNPC	0.1M KOH	16.48	-0.2 V	4.46	[27]
$Cu_{1.81}S$	0.1 M KOH	2.19 μmol h^{-1} cm^{-2}	-0.1 V	14.1	[28]
Co/C-900	0.1 M KOH	4.66 μmol h^{-1} cm^{-2}	-0.3 V	11.53	[29]
Co-doped $FePS_3$ nanosheets	0.1 M KOH	90.6	-0.4	3.38	[30]
Co-doped porous g-C_3N_4	0.1 M KOH	49.69	-0.1	32.20	[31]
CoFe double hydroxide	KOH	0.1 × 10^{-9} mol s^{-1} cm^{-2}	-1.1 V (vs. Hg/HgO)	14.18	[32]
Fe–S–C	0.1 M KOH	8.8 ± 1.3 μg h^{-1} mg^{-1}	-0.1 V	6.1 ± 0.9%	[33]
MoO_{2+x}	0.1 M KOH	3.95 μg $mg_{cat}^{-1}h^{-1}$	-0.2 V	22.1	[34]
Co_2B (1:8)	**0.1 M KOH**	**2980.22**	**-0.3 V**	**20.45**	**This work**

Table S1B. Comparison of NH_3 yield obtained from IC, Nessler's reagent and Indophenol blue method.

Method	**Yield rate (μg h^{-1} $mg^{-1}_{cat.}$)**
Indophenol blue	2980.22
Nessler's reagent	2346.63

Table S2A. Calculations of different parameters extracted from EIS in Fig. 1c for Co_2B (1:4/1:8/1:12) in N_2-saturated 0.1 M KOH.

Catalyst	**R_s (Ω)**	**R_p (Ω)**	**R_{ct} (Ω)**
Co_2B (1:4)	24.07	66.34	42.27
Co_2B (1:8)	23.17	61.83	38.83
Co_2B (1:12)	25.16	69.97	44.81

Table S2B. Values of C_{dl}, ECSA and roughness factor for catalysts in this study extracted from Fig. S6 respectively.

Catalyst	**C_{dl} (μF)**	**ECSA (cm^2)**	**Roughness factor (a.u.)**
Co_2B (1:4)	146	3.65	116.24
Co_2B (1:8)	420	10.5	334.39
Co_2B (1:12)	121	3.025	96.33

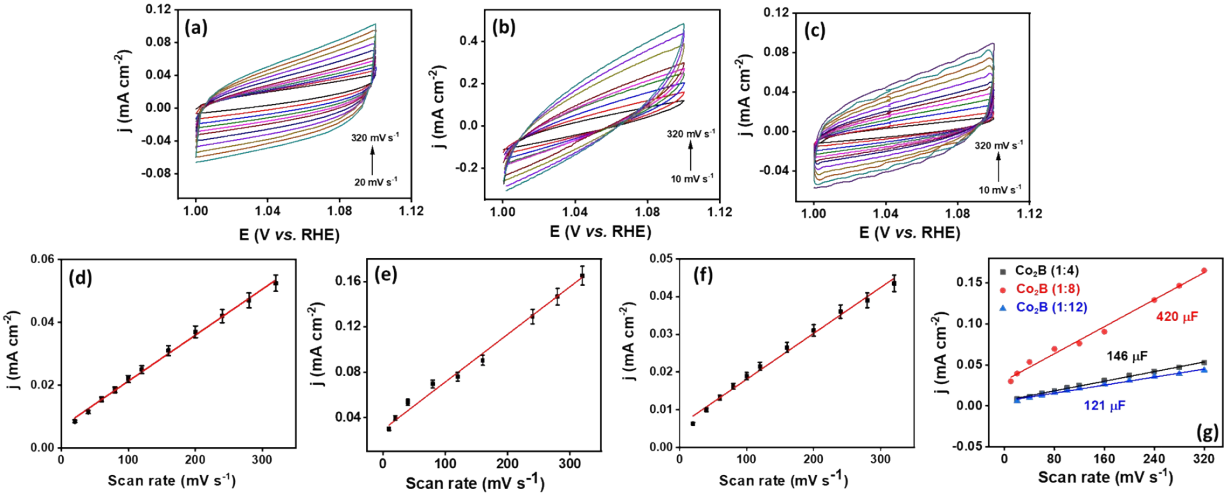

Fig. S7 Cyclic voltammograms in non-faradaic region for (a) Co_2B (1:4), (b) Co_2B (1:8) and (c) Co_2B (1:12) and simultaneous scan rate *vs.* current density plots (e)-(f) in N_2-saturated 0.1 M KOH. (g) Scan rate *vs.* current density plots showing C_{dl} values of Co_2B catalysts.

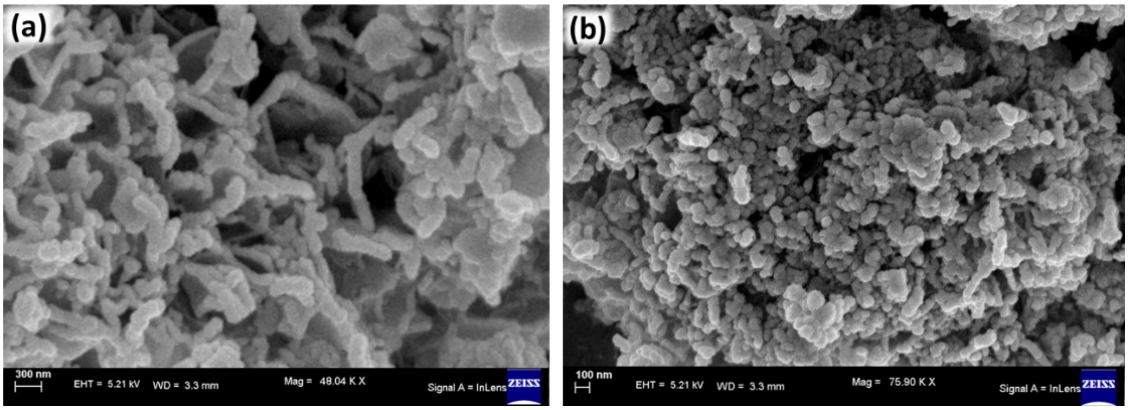

Fig. S8A FE-SEM images of (a) Co_2B (1:4) and (b) Co_2B (1:12) at different magnifications.

Table S2C. BET calculations for Co_2B catalysts.

S.No.	Catalyst	BET surface area ($m^2\ g^{-1}$)
1.	Co_2B (1:4)	73.2
2.	Co_2B (1:8)	103
3.	Co_2B (1:12)	34.1

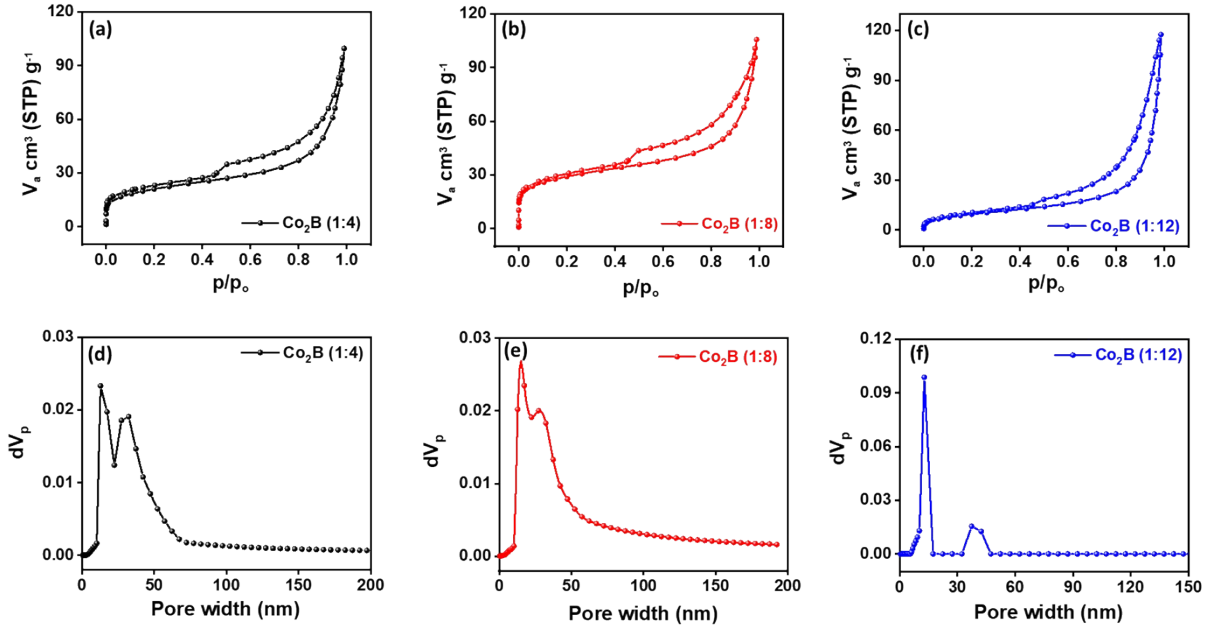

Fig. S8B (a)-(c) N_2 adsorption/desorption isotherms and (d)-(f) Pore size distribution for Co_2B catalysts respectively.

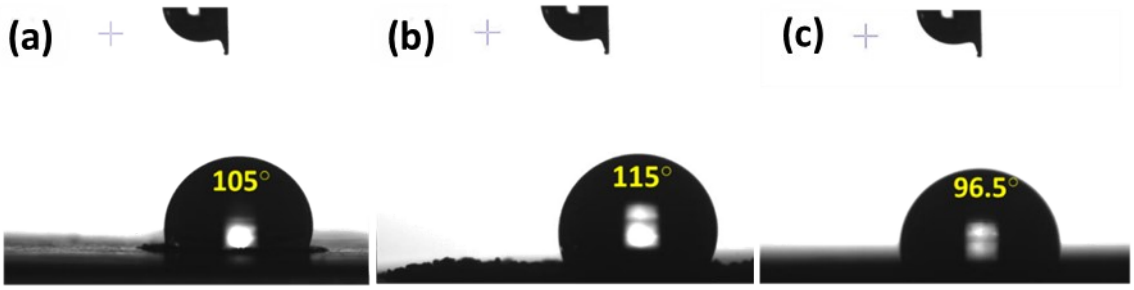

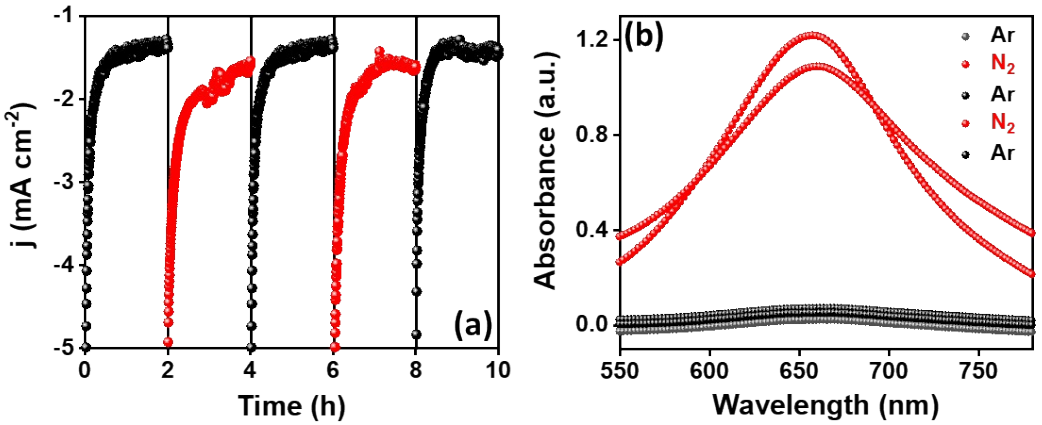

Fig. S8C Water contact angle images of (a) Co_2B (1:4), (b) Co_2B (1:8) and (c) Co_2B (1:12) respectively.

Fig. S9 (a) Chronoamperometric curves obtained for Co_2B (1:8) at -0.3 V *vs.* RHE in switching gas feed environments and (b) respective absorbance values obtained after quantification by Indophenol blue method.

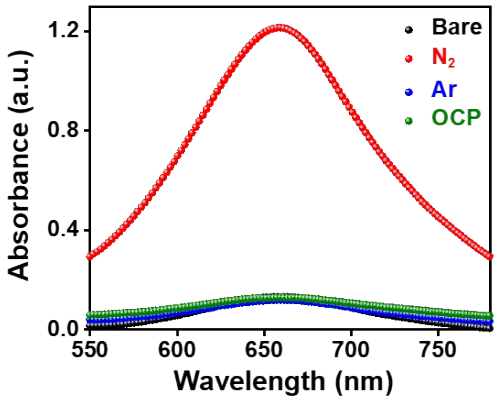

Fig. S10 Absorbance values obtained for Co_2B (1:8) after quantification during control experiments in Ar-saturated electrolyte, bare electrode and at open circuit potential.

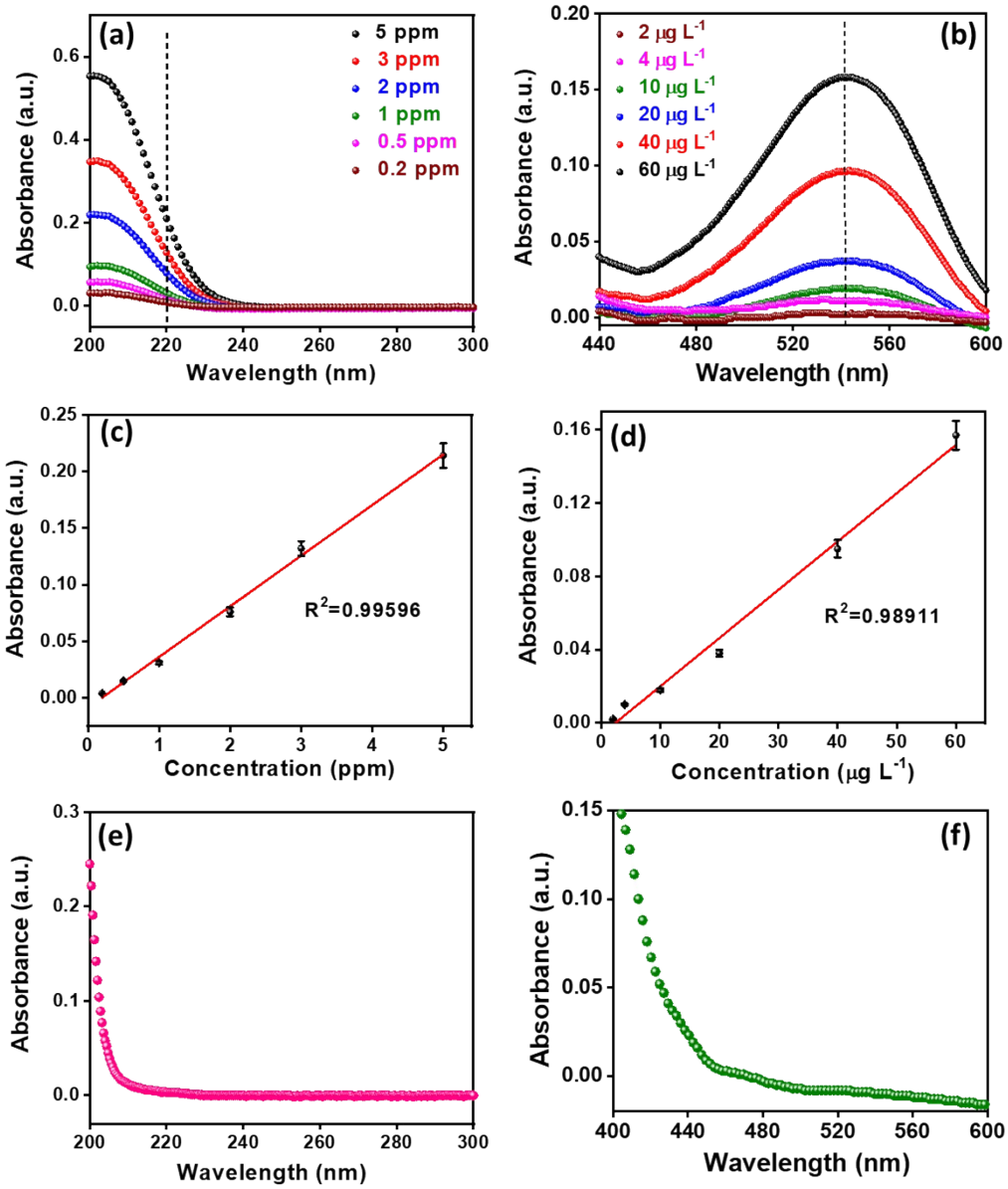

Fig. S11 UV-Vis. absorbance curves for standard (a) nitrate and (b) nitrite solutions with different concentrations and (c)-(d) respective calibration curves obtained from the same. Quantification of (e) nitrate and (f) nitrite in Co_2B (1:8) during NRR.

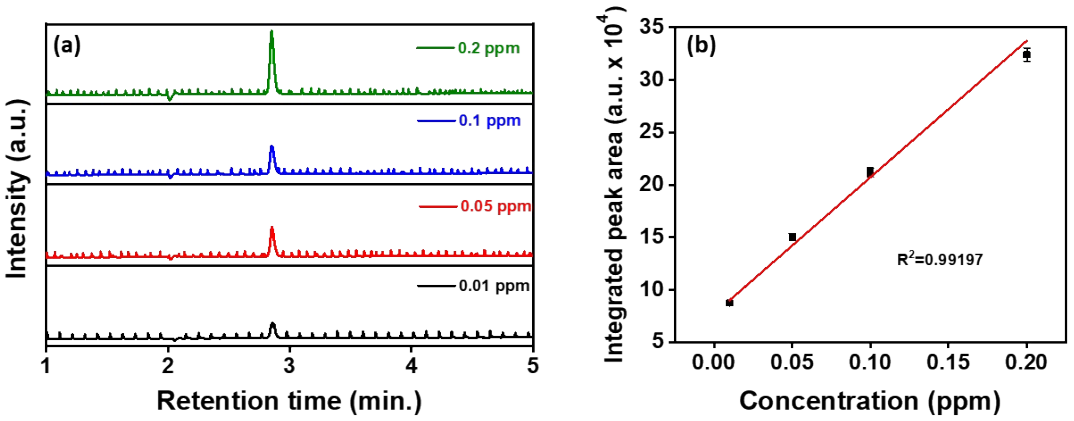

Fig. S12A Chromatogram for standard N_2O gas of different concentrations (0.01 ppm to 0.2 ppm) after analysis in SIM mode (m/z=44) in GC-MS and (b) standard calibration curve extracted from the same for N_2O quantification.

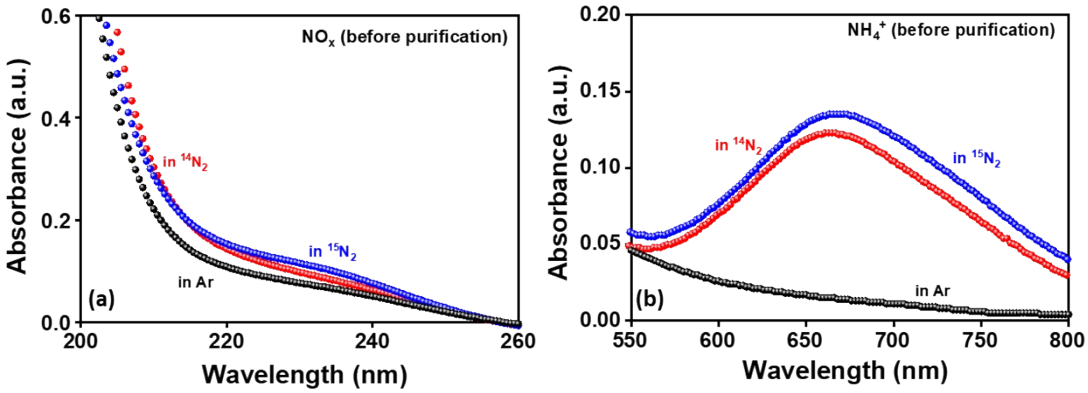

Fig. S12B UV-Vis. absorbance curves obtained before passing gas-supplies ($Ar/^{14}N_2/^{15}N_2$) through the (a) alkaline $KMnO_4$ solution to trap NO_x impurities and (B) acid trap to test NH_4^+ impurities.

Table S3. Quantified amounts of NO_x/NH_4^+ impurities before and after purification by scrubbing solution by colorimetric and GC-MS method.

S.No.	Gas supply	Before purification			After purification		
		NO/NO_2 (UV-Vis. spectroscopy)	N_2O (GC-MS)	NH_4^+ (UV-Vis. spectroscopy)	NO/NO_2 (UV-Vis. spectroscopy)	N_2O (GC-MS)	NH_4^+ (UV-Vis. spectroscopy)
1.	Ar (99.99%, Sigma)	0.6 ppm	<0.01 ppm	-	-	NA	NA
2.	$^{14}N_2$ (99.99% Sigma)	1.1 ppm	0.06 ppm	0.09 ppm	<0.01 ppm	<0.01 ppm	-
3.	$^{15}N_2$ (98%, Sigma)	1.2 ppm	0.07 ppm	0.08 ppm	<0.01 ppm	<0.01 ppm	-

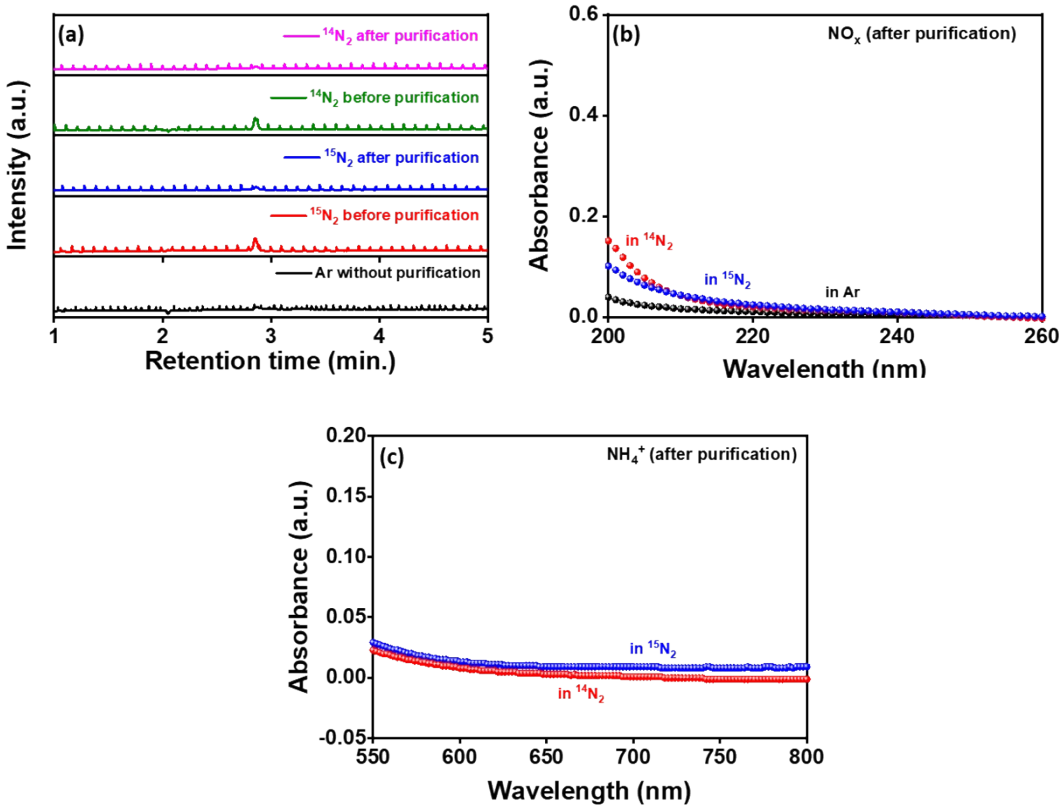

Fig. S13 (a) Chromatograms for Ar/$^{14}N_2$/$^{15}N_2$ gas-supplies before and after purification for N_2O quantification. UV-Vis. absorbance curves obtained after passing gas-supplies (Ar/$^{14}N_2$/$^{15}N_2$) through the (b) alkaline $KMnO_4$ solution to trap NO_x impurities and (c) acid trap to test NH_4^+ impurities.

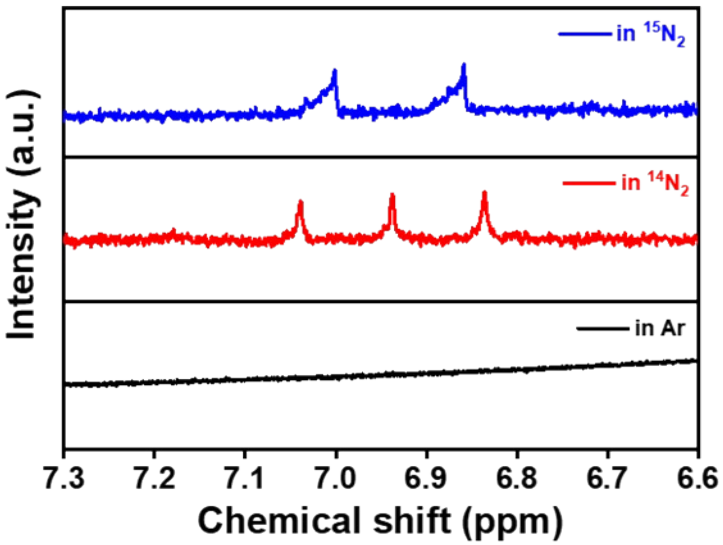

Fig. S14 ^{1}H-NMR spectrum acquired after 2 h isotope labelling NRR experiment by Co_2B (1:8) under different gas-supply (Ar/$^{14}N_2$/$^{15}N_2$) saturated electrolyte solutions.

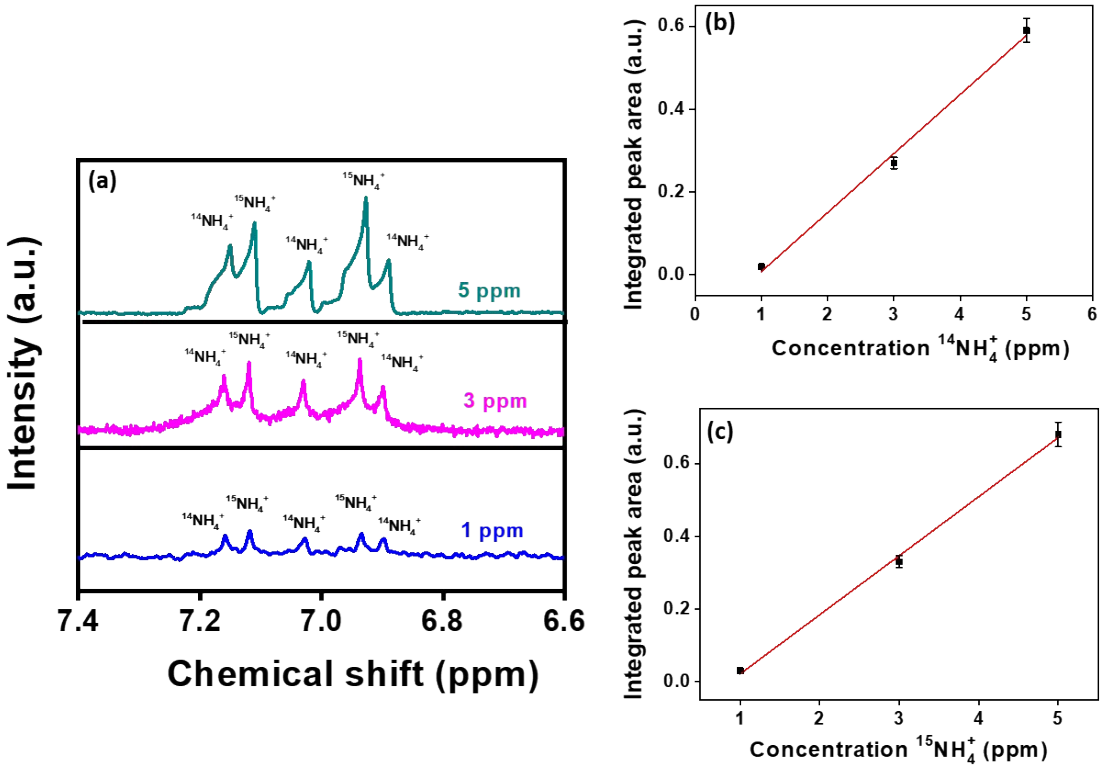

Fig. S15A Standard calibration curve extracted from ^{1}H-NMR spectrum (a) for (b) $^{14}NH_4^+$ and (c) $^{15}NH_4^+$ solutions with varying concentrations.

Table S4. Comparison of NH_3 yield rates obtained after NRR isotope labelling experiments by Co_2B (1:8) catalyst via different quantification methods.

S.No.	Quantification method	$^{14}NH_4^+$ yield rate (mg h^{-1} $mg_{cat.}^{-1}$)	$^{15}NH_4^+$ yield rate (mg h^{-1} $mg_{cat.}^{-1}$)

1.	Indophenol blue	2.94	2.93
2.	^{1}H-NMR spectroscopy	2.94	2.93
3.	Liquid chromatography-mass spectroscopy	2.98	2.95

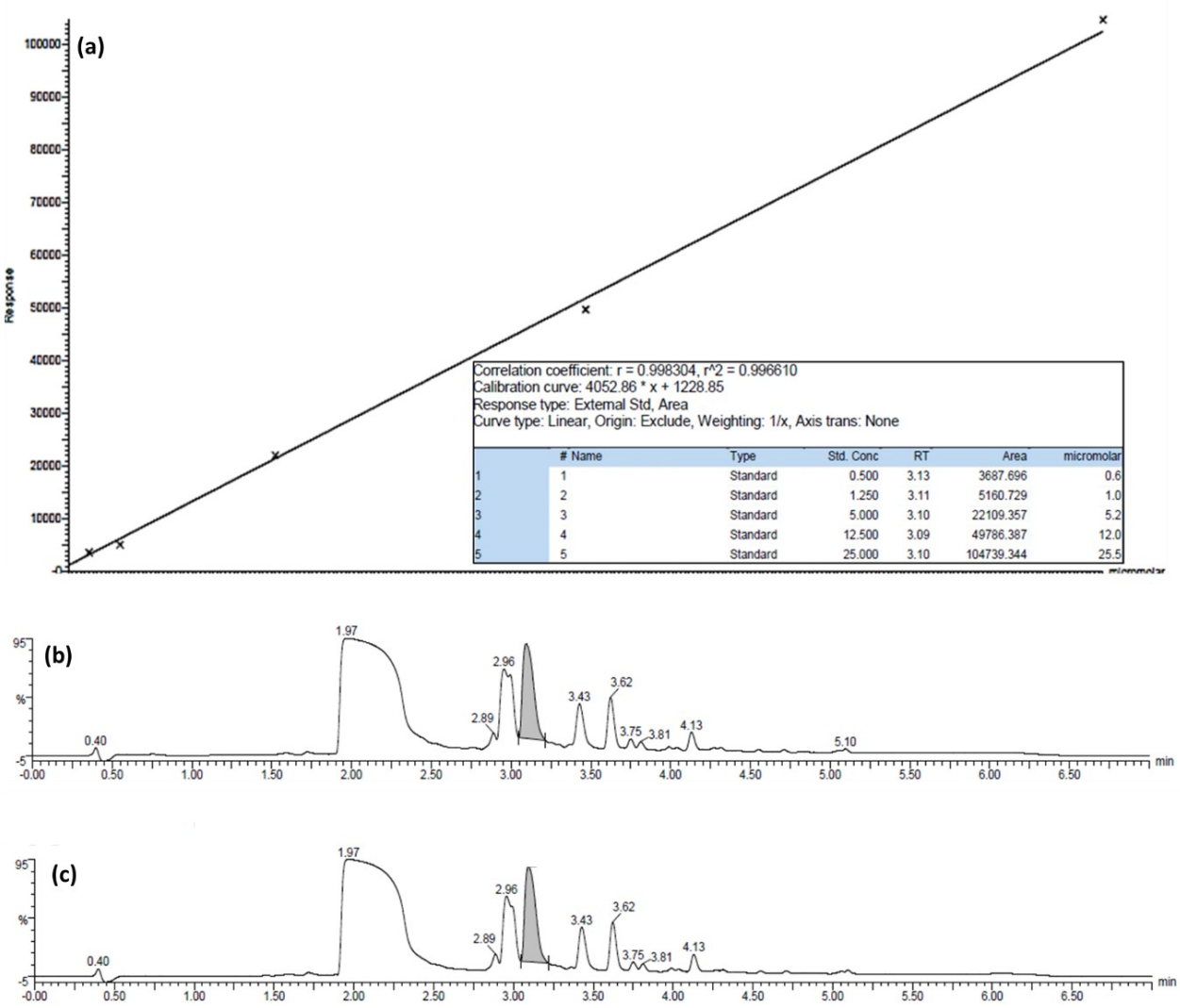

Fig. S15B (a) Standard calibration curve obtained for standard Indophenol red solutions with varying concentrations (0.1 to 5 ppm), liquid chromatogram for electrolyte solution after NRR performed in (a) $^{14}N_2$- and (b) $^{15}N_2$-saturated 0.1 M KOH solution.

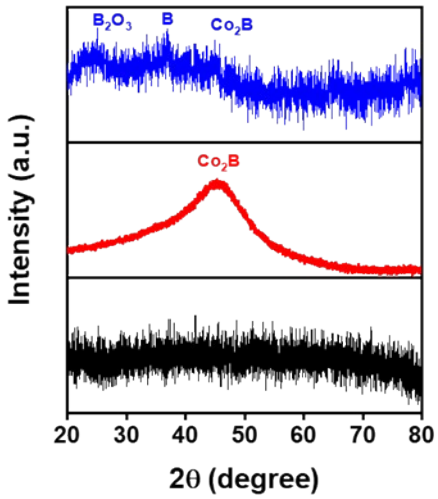

Fig. S16A Powder X-ray diffraction patterns of Co_2B [black: Co_2B (1:4); red: Co_2B (1:8); blue: Co_2B (1:12)].

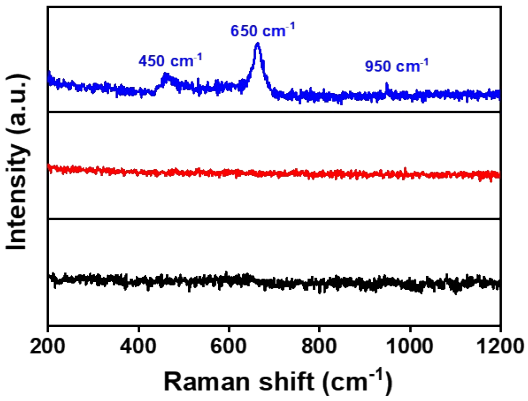

Fig. S16B Raman spectrum for Co_2B catalysts.

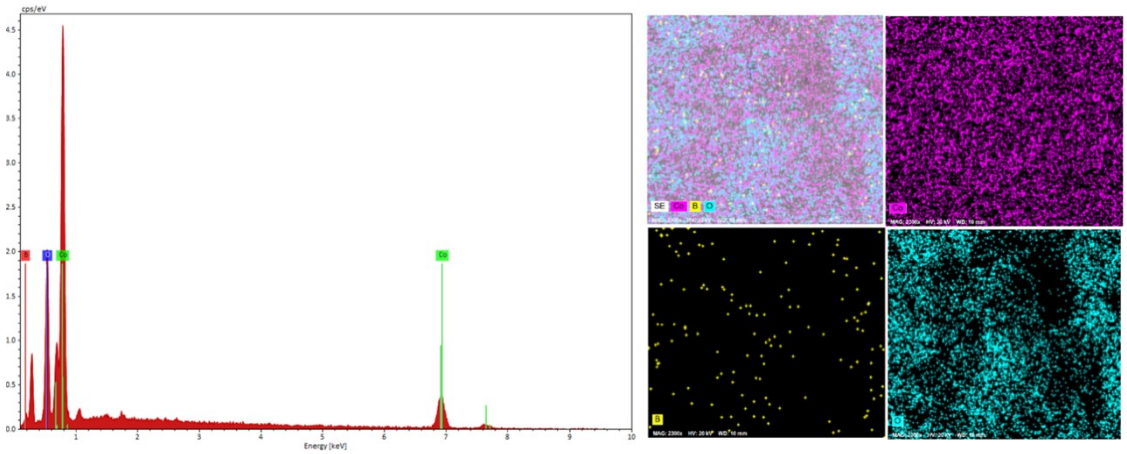

Fig. S17 EDS spectra and dot mapping analysis for Co_2B (1:8) catalyst.

Table S5A. EDS Composition analysis (at.%) for Co_2B (1:8).

Catalyst	Cobalt	Boron	Oxygen
Co_2B (1:8)	47.76	26.07	26.17

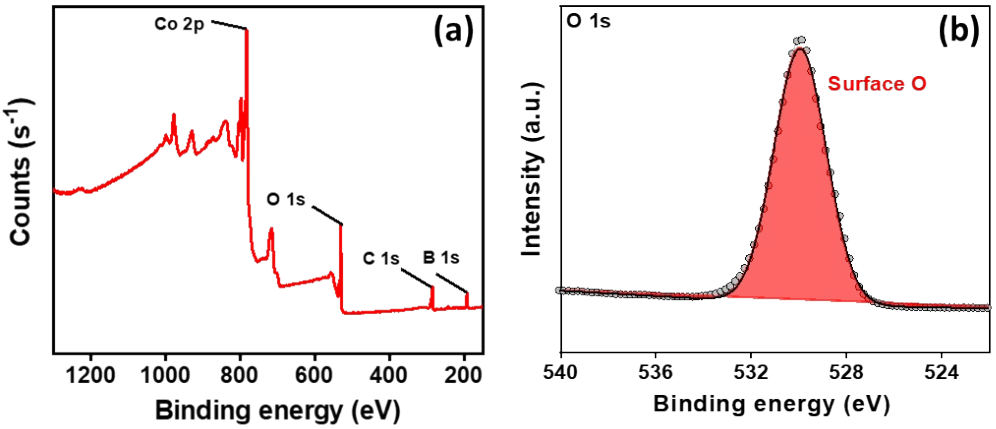

Fig. S18 (a) XP survey spectrum and (b) O 1s deconvoluted XP spectrum of Co_2B (1:8).

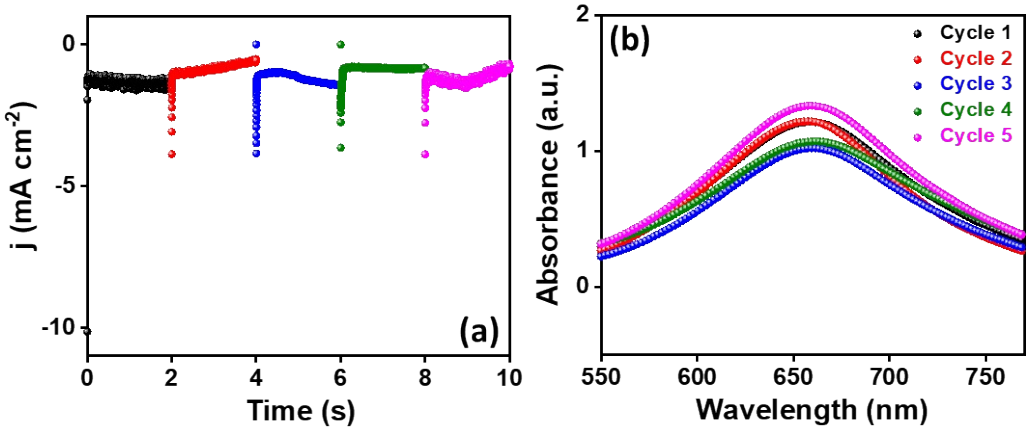

Fig. S19 (a) Chronoamperometric curves obtained for Co_2B (1:8) at -0.3 V *vs.* RHE for 10 h and (b) respective absorbance values obtained after quantification by Indophenol blue method.

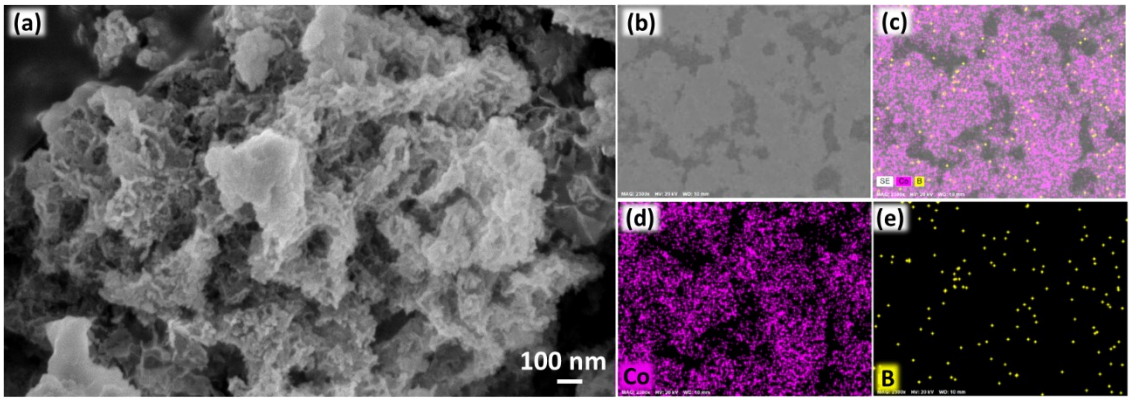

Fig. S20 (a) SEM image and (b-e) EDS dot mapping showing presence of both Co and B for Co_2B (1:8) after stability test for NRR.

Computational Methodology

We have carried out density functional theory (DFT) based electronic structure calculations[35, 36] using Vienna *ab-initio* simulation package (VASP) code throughout the theoretical investigation.[37] The projector augmented-wave (PAW) formalism[38] is used, while the exchange and correlation potential is described through generalized gradient approximation using Perdew- Burke-Ernzerhof (PBE) functional[39] The kinetic energy cut-off corresponding to the plane wave basis set has been used as 500 eV. All the surface configurations along with the surface-adsorbate systems are fully relaxed while achieving the minimum-energy criteria until the Hellman-Feynman forces become less than 0.01 eV/Å. We have constructed the Co_2B surface along [001] direction while considering 15 Angstrom vacuum along z-direction, which will remove the interaction between periodic images. The Brillouin zone has been sampled using 5×5×1 Monkhorst-Pack k- mesh for structural optimization for surface calculations.[40]

Table S5B. Adsorption free energy values calculated from DFT model for NRR over "**Co"** in Co_2B (1:8) catalyst.

Structure	**$E_{surface+adsorbate}$ (eV)**	**$E_{Surface}$ (eV)**	**$E_{adsorbate}$ (eV)**	**$E_{adsorption\ energy}$ (eV)**	**$\Delta G_{Free\ energy}$ (eV) at 0 V**	**$\Delta G_{Free\ energy}$ (eV) at -0.3 V**
N_2^* on Co	-166.206473	-145.05757	-16.657685	-4.4912184	-4.9322184	-4.6322184
N_2H^* on Co	-171.4847209	-145.05757	-18.017425	-8.4097255	-8.0487255	-7.7487255
$N_2H_2^*$ on Co	-172.6671155	-145.05757	-21.084547	-6.5249982	-6.2349982	-5.9349982
N^* on Co	-160.8272799	-145.05757	-8.3288429	-7.4408675	-7.6218675	-7.3218675
NH^* on Co	-159.9010614	-145.05757	-8.1026962	-6.7407957	-6.64779574	-6.34779574
NH_2^* on Co	-167.6530729	-145.05757	-13.525779	-9.0697238	-8.67172382	-8.37172382
NH_3^* on Co	-169.5893949	-145.05757	-19.533373	-4.99845196	-4.16145196	-3.86145196
H^* on Co	-156.1036094	-145.05757	-3.3852118	-7.660828035	-7.42082803	-7.12082803

To support the adsorption of NRR intermediates on the Co site, another adsorption has been performed on the B site. The outcomes show that the N_2 adsorption process is more favorable on the Co site.

Table S5C. Adsorption free energy values calculated from DFT model for NRR over "**B"** in Co_2B (1:8) catalyst.

Structure	**E surface + adsorbate (eV)**	**E Surface (eV)**	**E adsorbate (eV)**	**E adsorption energy (eV)**	**ΔG Free energy (eV) at 0 V**	**ΔG Free energy (eV) at -0.3 V**
N_2^* on B	-162.410528	-145.05757	-16.657685	-0.6952734	-1.1362734	-0.8362734
N_2H^* on B	-168.495766	-145.05757	-18.017425	-5.4207707	-5.0597707	-4.7597707
$N_2H_2^*$ on B	-170.536490	-145.05757	-21.084547	-4.3943734	-4.1043734	-3.8043734
N^* on B	-157.563482	-145.05757	-8.3288429	-4.1770703	-4.3580703	-4.0580703
NH^* on B	-159.854048	-145.05757	-8.1026962	-6.6937823	-6.6007823	-6.3007823
NH_2^* on B	-165.919044	-145.05757	-13.525779	-7.3356955	-6.9376955	-6.6376955
NH_3^* on B	-166.713559	-145.05757	-19.533373	-2.1226165	-1.2856165	-0.9856165
H^* on B	-153.040994	-145.05757	-3.3852118	-4.5982128	-4.3582128	-4.0582128

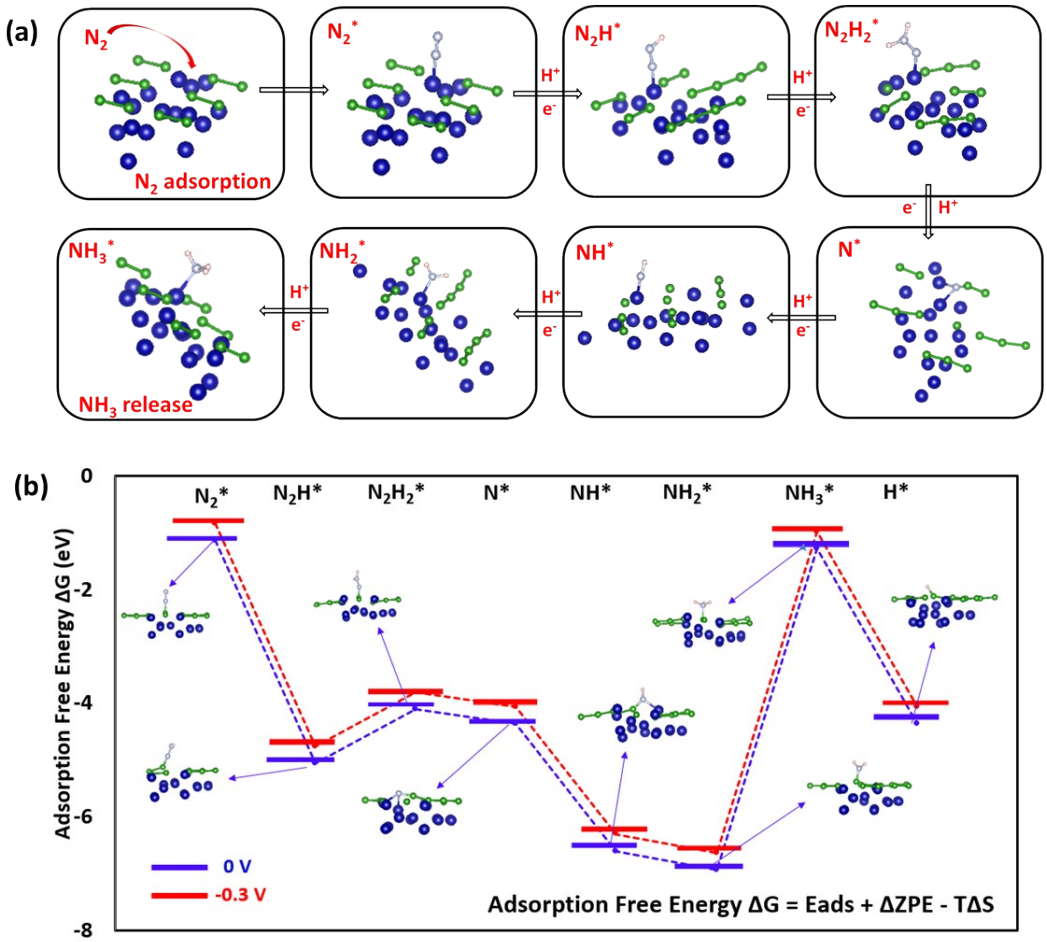

Fig. S21 (a) Optimized configurations of different reaction intermediates during NRR on Co sites of Co_2B surface via end-on adsorption and (b) Reaction coordinate corresponding to N_2 reduction to NH_3 on B site of Co_2B catalyst surface.

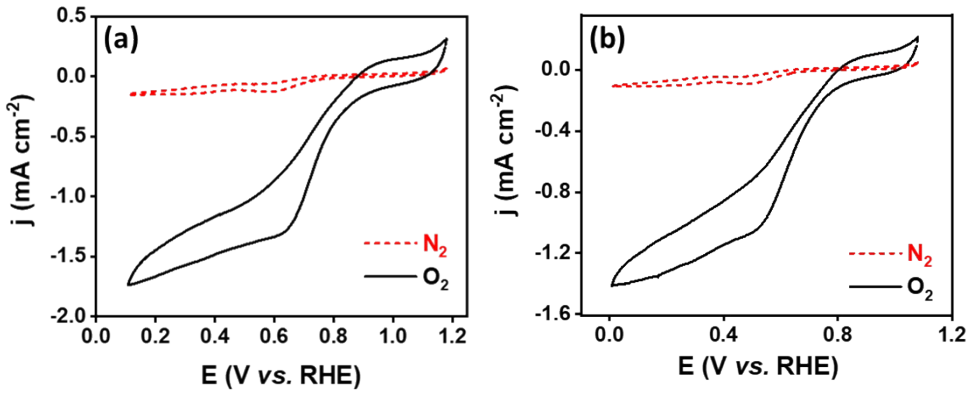

Fig. S22 Cyclic voltammograms of (a) Co_2B (1:4) and (b) Co_2B (1:12) in N_2- and O_2- saturated 0.1 M KOH electrolyte solution.

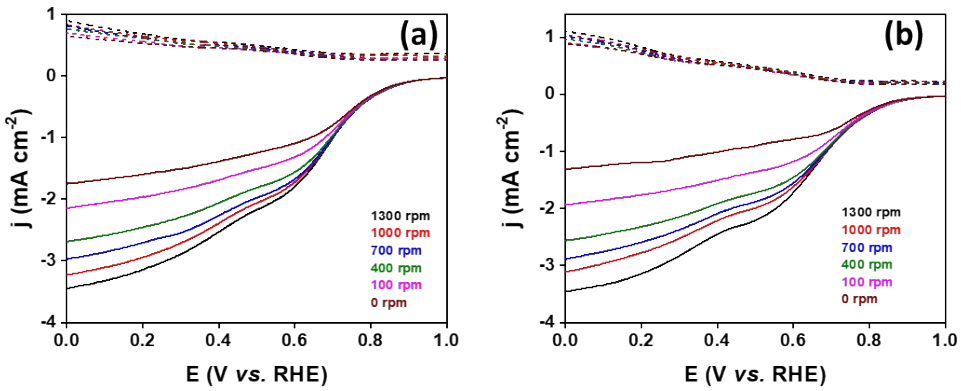

Fig. S23 RDE polarization curves of (a) Co_2B (1:4) and (b) Co_2B (1:12) during ORR at different rotation rates varying from 0 to 1300 rpm at a sweep rate of 5 mV s^{-1}.

Table S6A. ORR performance comparison of Co_2B catalysts in O_2-saturated 0.1 M KOH electrolyte solution.

Catalyst	**Onset potential$_{@-0.1\ mA\ cm^{-2}}$**	**Half wave potential**	**Current density (at 0.2 V)**
Co_2B (1:4)	0.89 V	0.69 V	-3.37 mA cm^{-2}
Co_2B (1:8)	0.98 V	0.83 V	-4.9 mA cm^{-2}
Co_2B (1:12)	0.86 V	0.66 V	-3.38 mA cm^{-2}

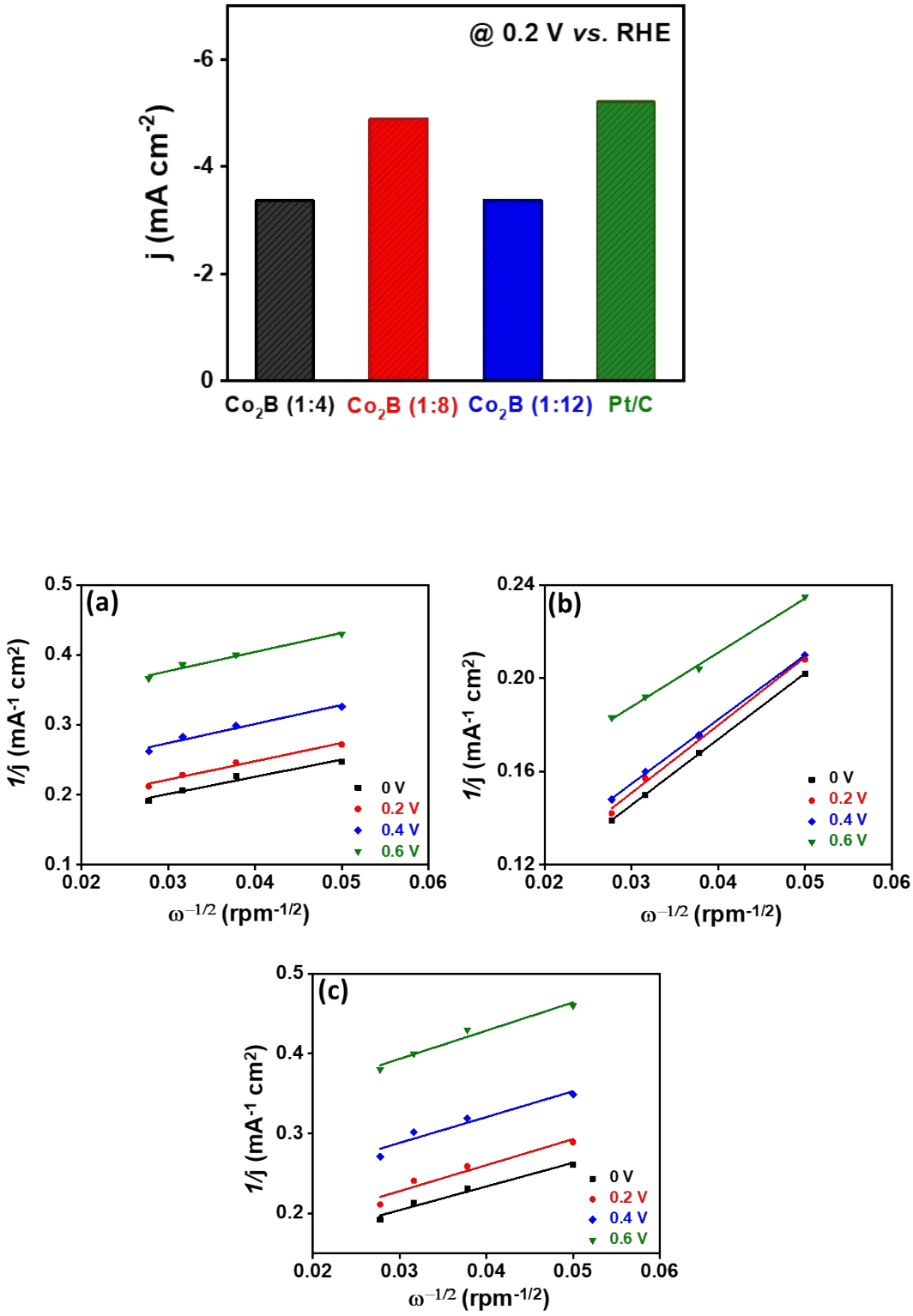

Fig. S24 Bar diagram comparison for diffusion limited current density during ORR.

Fig. S25 Koutecky-Levich plots derived from corresponding LSV of (a) Co_2B (1:4), (b) Co_2B (1:8), and (c) Co_2B (1:12) respectively.

Table S6B. Total number of electrons transferred and simultaneous H_2O_2 production during ORR by Co_2B catalysts.

Catalyst	n (O_2)				H_2O_2 (%)			
	0 V	0.2 V	0.4 V	0.6 V	0 V	0.2 V	0.4 V	0.6 V
Co_2B (1:4)	3.6	3.7	3.71	2.892	20.19	14.51	14.07	55.38
Co_2B (1:8)	3.83	3.841	3.843	3.86	8.42	7.91	7.76	6.81
Co_2B (1:12)	3.63	3.637	3.65	3.71	18.34	18.35	17.02	14.4

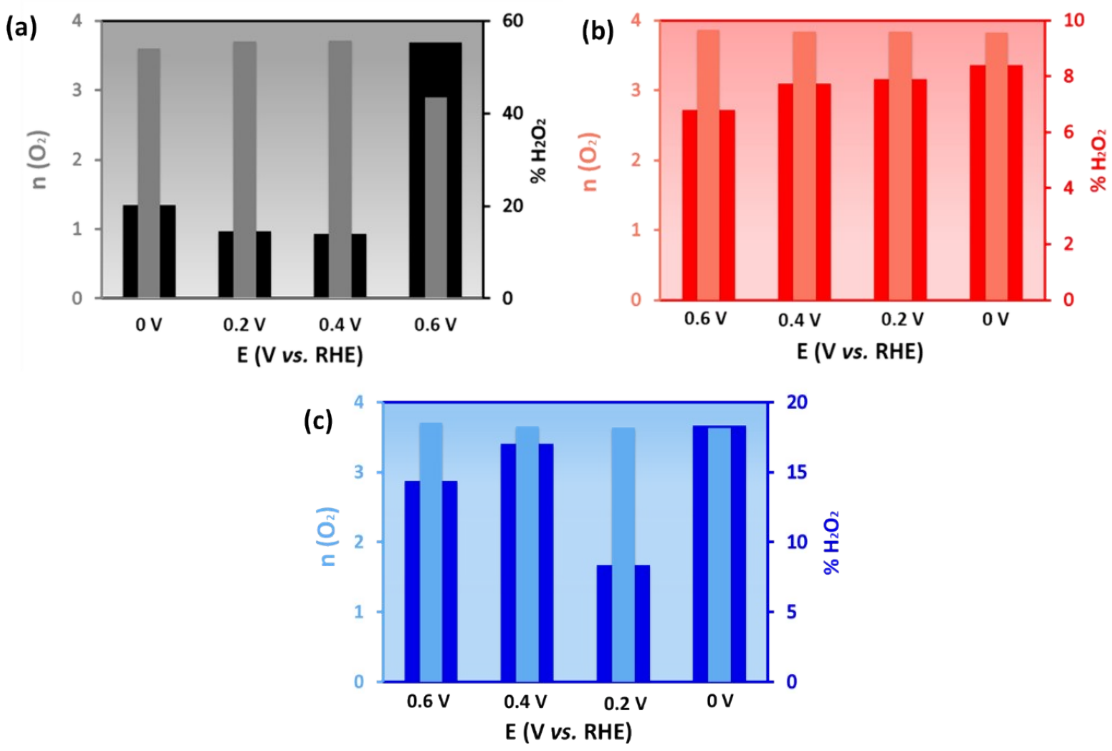

Fig. S26 Bar diagram representation of H_2O_2 (%) and no. of electrons transferred during ORR by (a) Co_2B (1:4), (b) Co_2B (1:8), and (c) Co_2B (1:12).

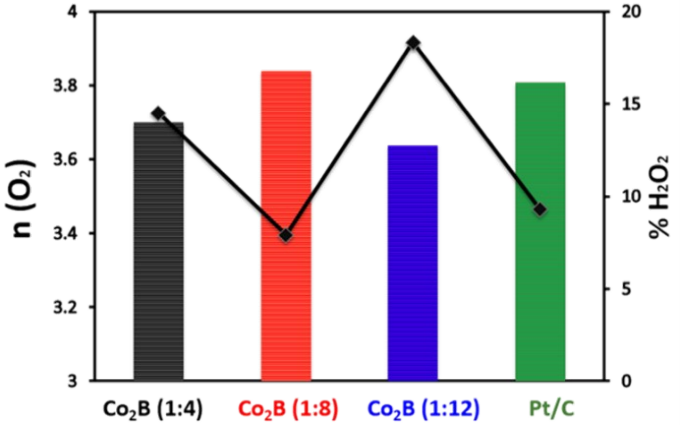

Fig. S27 Bar diagram comparison of no. of electrons and H_2O_2 produced by catalysts @ 0.2 V.

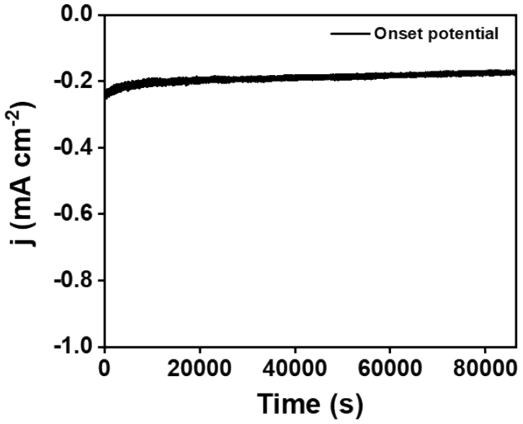

Fig. S28 Stability test performed for Co_2B (1:8) in O_2-saturated 0.1 M KOH for 24 h at a fixed ORR onset potential.

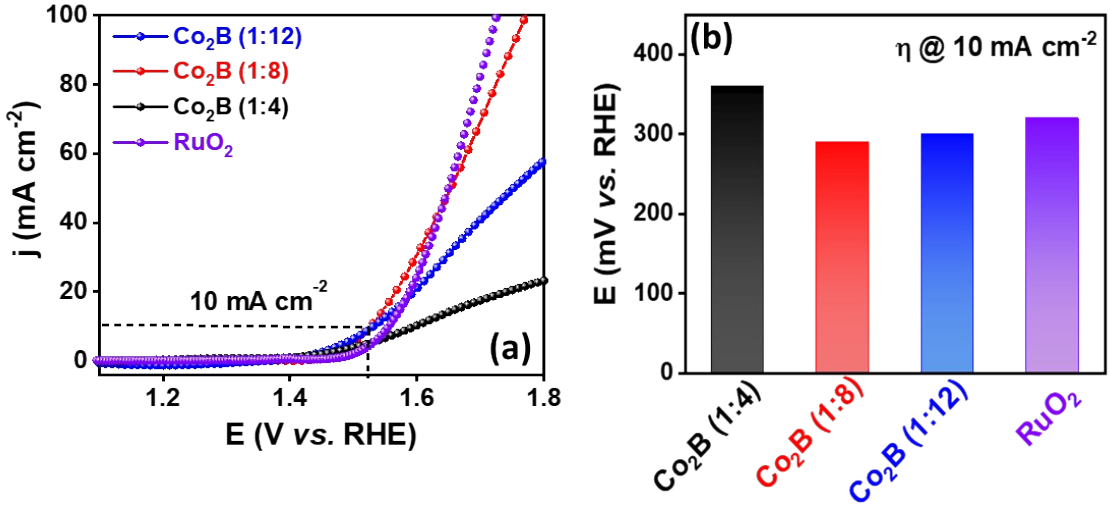

Fig. S29 (a) LSV polarization curves during OER for variants of Co_2B and benchmark RuO_2 catalyst at 10 mV s^{-1} and (b) Bar diagram represnting the comparison of overpotential required by catalysts to reach 10 mA cm^{-2} current density.

Table S7. OER performance comparison of Co_2B catalysts in O_2-saturated 0.1 M KOH electrolyte solution.

Catalyst	Overpotential (η at 10 mA cm^{-2})	Current density (at 1.75 V *vs.* RHE)	Tafel slope (mV dec^{-1})
Co_2B (1:4)	350 mV	20 mA cm^{-2}	207
Co_2B (1:8)	290 mV	92.5 mA cm^{-2}	80
Co_2B (1:12)	300 mV	51 mA cm^{-2}	126

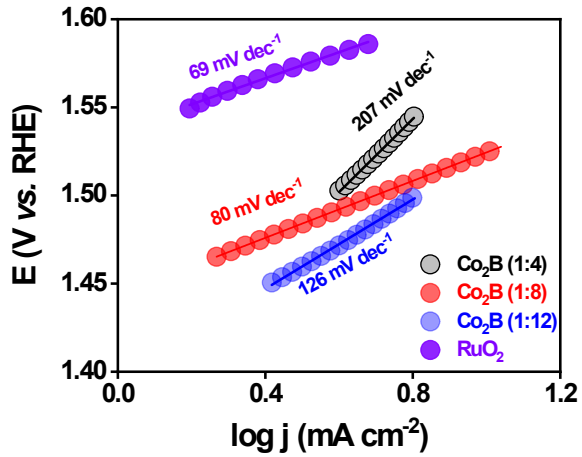

Fig. S30 Tafel plots derived from Fig. S29a for different catalysts during OER.

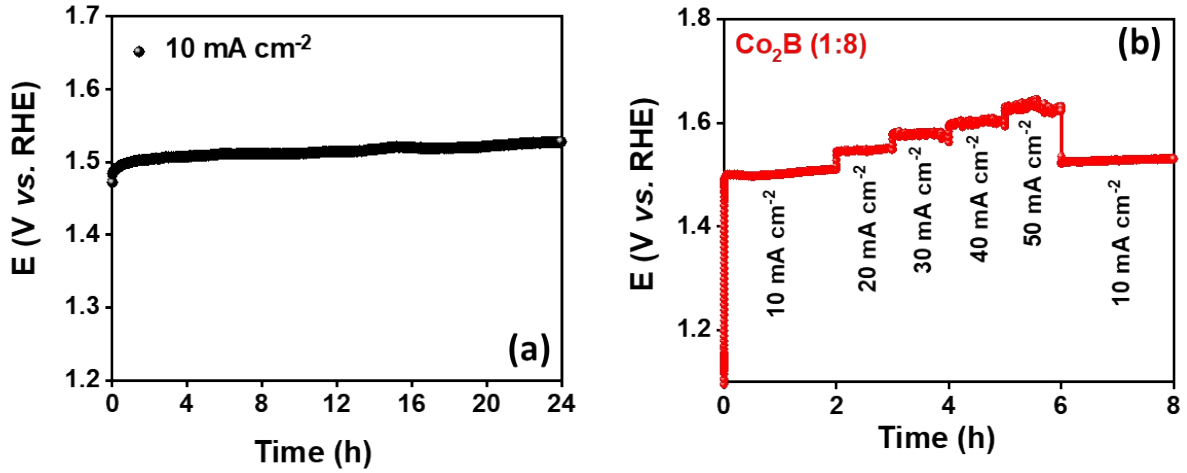

Fig. S31 (a) Stability tests performed for Co_2B (1:8) for 24 h at 10 mA cm^{-2} current density during OER and (b) Sequential chronopotentiometry performed at different current densities between 10-50 mA cm^{-2} for Co_2B (1:8).

Table S8. Comparison of bifunctional activity of Co_2B catalysts and benchmark catalysts for ORR/OER.

Catalyst	OER overpotential ($E_{j=10\ mA\ cm^{-2}}$)	ORR half-wave potential ($E_{ORR1/2}$)	Potential gap ($\Delta E = E_j - E_{ORR1/2}$)
Co_2B (1:4)	1.58 V	0.69 V	0.89
Co_2B (1:8)	1.52 V	0.83 V	0.69
Co_2B (1:12)	1.53 V	0.66 V	0.87
Pt/C	1.6 V	0.87 V	0.73
RuO_2	1.55 V	0.8 V	0.75

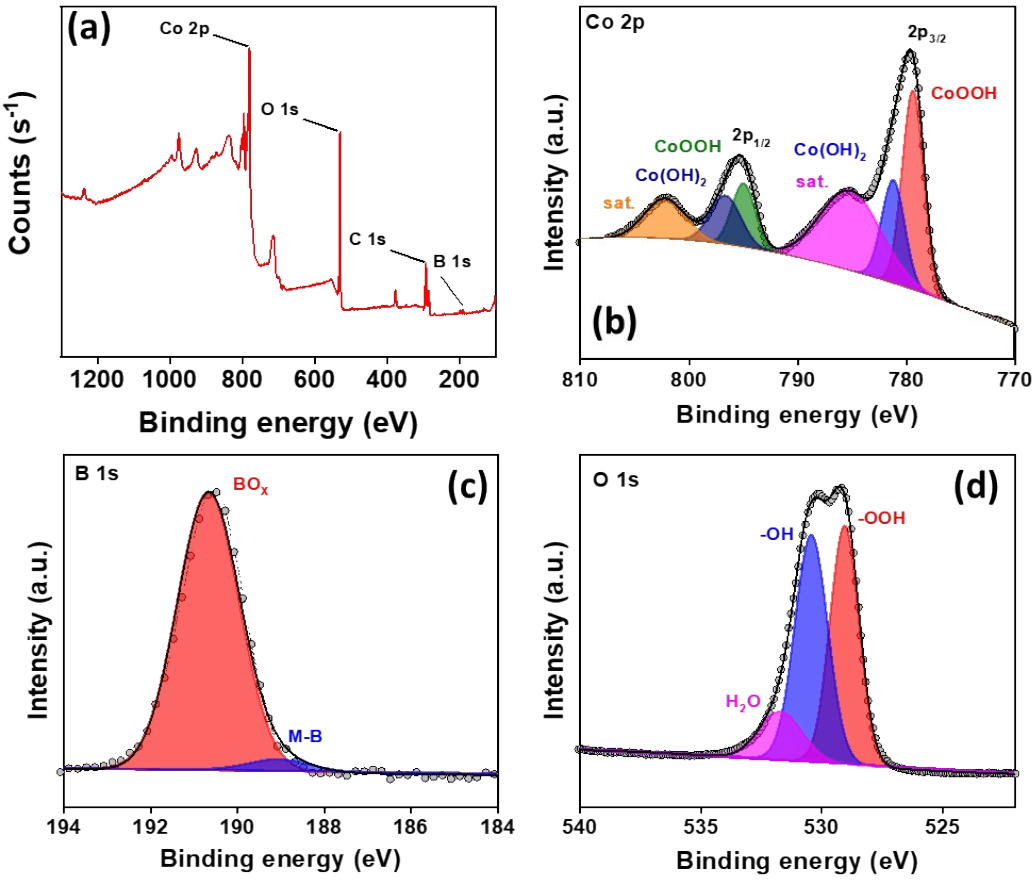

Fig. S32 (a) Survey spectrum, (b) Co 2p, (c) B 1s and (d) O 1s spectrum of Co_2B (1:8) after OER stability tests.

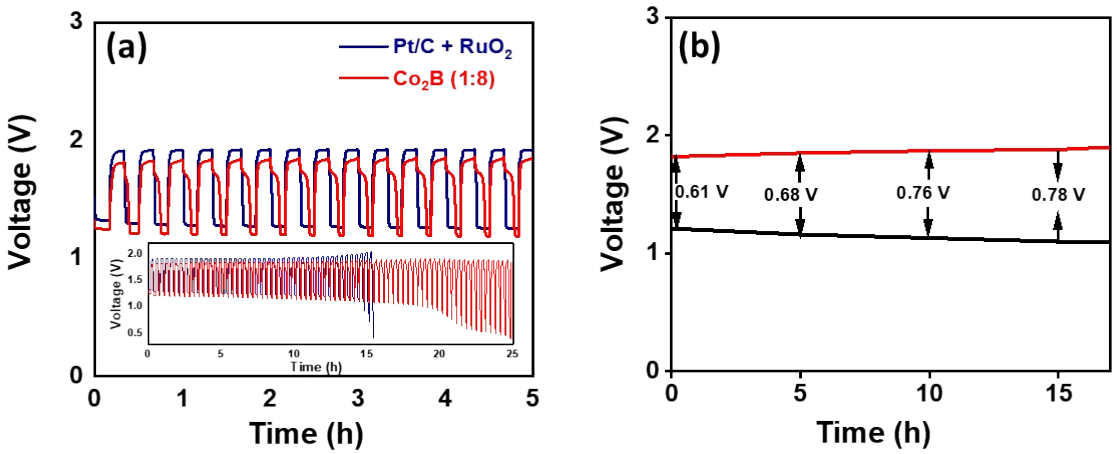

Fig. S33A (a) Galvanostatic charge-discharge cycling stability curves for Co_2B (1:8) and Pt/C+RuO_2 at 10 mA cm^{-2} current density (10 min. Charging-10 min. discharging) and (b) Potential gap variation on increased number of charge-discharge cycles during battery performance analysis.

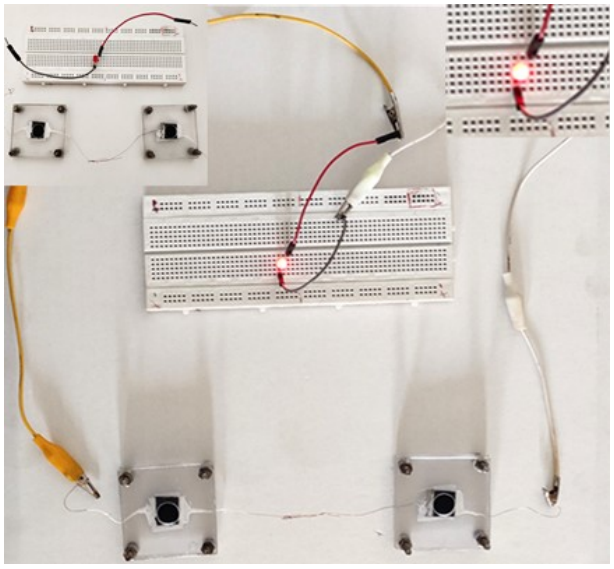

Fig. S33B Zn-air battery equipped with Co_2B (1:8) air cathode assembled in series to light a red LED of 2.0 V (Inset (left): no connection with battery; (right): lightened LED).

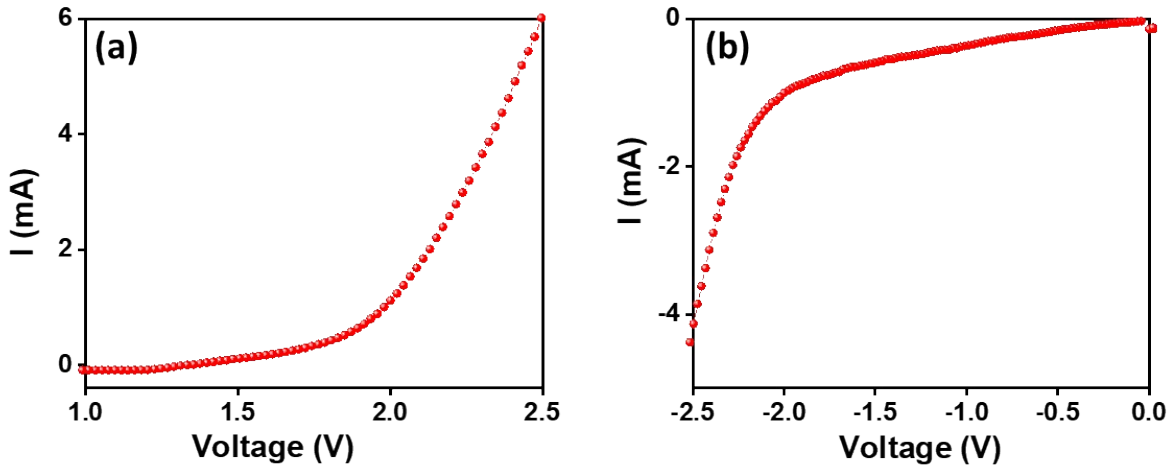

Fig. S34 LSV acquired under full-cell conditions for overall NH_3 synthesis (a) anodic sweep, (b) cathodic sweep, showing bifunctional activity of Co_2B (1:8) catalyst towards OER at anode and NRR at cathode.

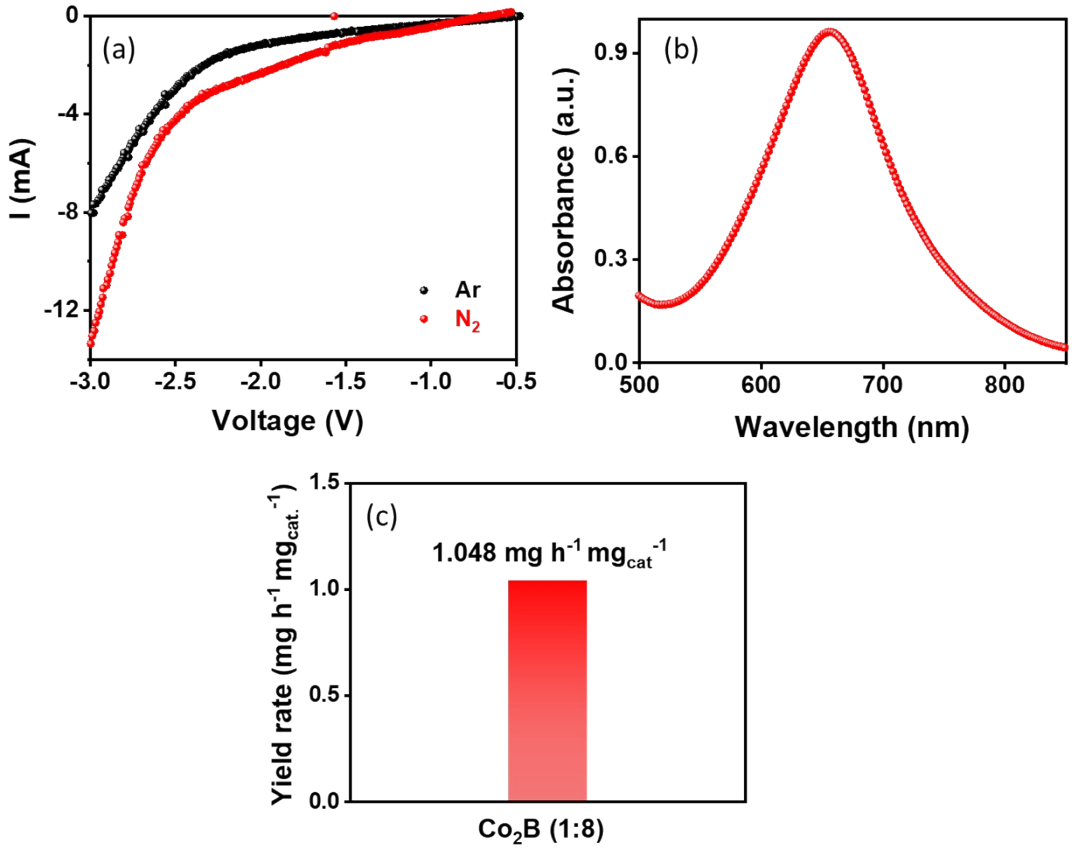

Fig. S35 (a) LSV for full-cell equipped with Co_2B (1:8) for NH_3 synthesis, (b) UV-vis curve obtained after quantification by Indophenol blue method and (c) NH_3 yield produced after 2 h of electrolysis by battery powered NH_3 production cell setup.

Table S9. Comparison of self-powered electrochemical ammonia synthesis over reported heterogeneous catalysts

S.No.	Power source	Power source efficiency				NH_3 cell setup							Ref.
		Catalyst	OCV (V)	Power density (mW cm^{-2})	Specific capacity (mAh g^{-1})	Half cell			Full cell				
						ν_{NH3} (μg h^{-1} mg^{-1})	F.E. (%)	Pot. (V *vs.* RHE)	Catalyst	Cathode	Anode	ν_{NH3}	
1.	Zn-air battery	Nitrogen-doped porous carbon[a]	1.35	-	-	1.31 mmol h^{-1} $g^{-1}_{cat.}$	9.98	-0.4	-	NPC-500	Carbon cloth	1.28 mmol h^{-1} $g^{-1}_{cat.}$	[41]
2.	Solid state Zn-air battery	Boron, nitrogen and fluorine ternary-doped carbon[a]	1.48	127	730 @ 5 mA cm^{-2}	41	14	-0.4	Bifunctional	BNF-C	BNF-C	-	[42]
3.	**Zn-air battery**	**Co_2B nanosheets[a]**	**1.45**	**500**	**889 @ 10 mA cm^{-2}**	**2980.22**	**20.45**	**-0.3**	**Bifunctional**	**Co_2B (1:8)**	**Co_2B (1:8)**	**1068 μg h^{-1} mg^{-1}_{cat} (2 h)**	Our work

[a]oxygen bifunctional catalyst

OCV: Open circuit voltage; F.E.: Faradaic efficiency; $\nu_{NH3.}$ NH_3 yield rate; NPC: Nitrogen-doped porous carbon; BNF-C: Boron, nitrogen and fluorine ternary-doped carbon; MSCM: melamine-sponge-based carbon materials; BN-CNF: Boron and nitrogen co-doped porous carbon nanofibers

References

1. L. Zhang, X. Ji, X. Ren, Y. Ma, X. Shi, Z. Tian, A. M. Asiri, L. Chen, B. Tang and X. Sun, *Adv. Mater.*, 2018, **30**, 1800191.
2. Y. Zhao, R. Shi, X. Bian, C. Zhou, Y. Zhao, S. Zhang, F. Wu, G. I. Waterhouse, L. Z. Wu and C. H. Tung, *Adv. Sci.*, 2019, **6**, 1802109.
3. A. C. Nielander, J. M. McEnaney, J. A. Schwalbe, J. G. Baker, S. J. Blair, L. Wang, J. G. Pelton, S. Z. Andersen, K. Enemark-Rasmussen and V. Colic, *ACS Catal.*, 2019, **9**, 5797-5802.
4. L. Li, C. Tang, D. Yao, Y. Zheng and S.-Z. Qiao, *ACS Energy Lett.*, 2019, **4**, 2111-2116.
5. H. Ren, Y. Pan, C. C. Sorrell and H. Du, *J. Mater. Chem. A*, 2020, **8**, 3154-3159.
6. Y. Fu, K. Li, M. Batmunkh, H. Yu, S. Donne, B. Jia and T. Ma, *ACS Appl. Mater. Interfaces*, 2020, **12**, 44830-44839.
7. W. Li, W. Fang, C. Wu, K. N. Dinh, H. Ren, L. Zhao, C. Liu and Q. Yan, *J. Mater. Chem. A*, 2020, **8**, 3658-3666.
8. T. Chen, S. Liu, H. Ying, Z. Li and J. Hao, *Chem. Asian J.*, 2020, **15**, 1081-1087.
9. W. Zang, T. Yang, H. Zou, S. Xi, H. Zhang, X. Liu, Z. Kou, Y. Du, Y. P. Feng and L. Shen, *ACS Catal.*, 2019, **9**, 10166-10173.
10. Y.-X. Lin, S.-N. Zhang, Z.-H. Xue, J.-J. Zhang, H. Su, T.-J. Zhao, G.-Y. Zhai, X.-H. Li, M. Antonietti and J.-S. Chen, *Nat. Commun.*, 2019, **10**, 1-7.
11. M. Wang, S. Liu, T. Qian, J. Liu, J. Zhou, H. Ji, J. Xiong, J. Zhong and C. Yan, *Nat. Commun.*, 2019, **10**, 341.
12. S. Mukherjee, D. A. Cullen, S. Karakalos, K. Liu, H. Zhang, S. Zhao, H. Xu, K. L. More, G. Wang and G. Wu, *Nano Energy*, 2018, **48**, 217-226.
13. L. Han, X. Liu, J. Chen, R. Lin, H. Liu, F. Lü, S. Bak, Z. Liang, S. Zhao and E. Stavitski, *Angew. Chem.*, 2019, **131**, 2343-2347.

14. H. Wang, Y. Li, C. Li, K. Deng, Z. Wang, Y. Xu, X. Li, H. Xue and L. Wang, *J. Mater. Chem. A*, 2019, **7**, 801-805.
15. F. Pang, Z. Wang, K. Zhang, J. He, W. Zhang, C. Guo and Y. Ding, *Nano Energy*, 2019, **58**, 834-841.
16. H.-M. Liu, S.-H. Han, Y. Zhao, Y.-Y. Zhu, X.-L. Tian, J.-H. Zeng, J.-X. Jiang, B. Y. Xia and Y. Chen, *J. Mater. Chem. A*, 2018, **6**, 3211-3217.
17. Y. Yang, L. Zhang, Z. Hu, Y. Zheng, C. Tang, P. Chen, R. Wang, K. Qiu, J. Mao and T. Ling, *Angew. Chem. Int. Ed.*, 2020, **59**, 4525-4531.
18. Y. Zhao, F. Li, W. Li, Y. Li, C. Liu, Z. Zhao, Y. Shan, Y. Ji and L. Sun, *Angew. Chem. Int. Ed.*, 2021, **60**, 20331-20341.
19. A. Liu, M. Gao, X. Ren, F. Meng, Y. Yang, Q. Yang, W. Guan, L. Gao, X. Liang and T. Ma, *Nanoscale*, 2020, **12**, 10933-10938.
20. A. Liu, X. Liang, Q. Yang, X. Ren, M. Gao, Y. Yang and T. Ma, *ChemPlusChem*, 2021, **86**, 166-170.
21. A. Liu, Q. Yang, X. Ren, M. Gao, Y. Yang, L. Gao, Y. Li, Y. Zhao, X. Liang and T. Ma, *Sustain. Energy Fuels*, 2020, **4**, 5061-5071.
22. W. Guo, Z. Liang, J. Zhao, B. Zhu, K. Cai, R. Zou and Q. Xu, *Small Methods*, 2018, **2**, 1800204.
23. H. Cheng, P. Cui, F. Wang, L. X. Ding and H. Wang, *Angew. Chem.*, 2019, **131**, 15687-15693.
24. G. Li, H. Lin, Z. Pan, Y. Liu and L. An, *Int. J. Energy Res.*, 2021, **45**, 19634-19644.
25. M. Bat-Erdene, G. Xu, M. Batmunkh, A. S. Bati, J. J. White, M. J. Nine, D. Losic, Y. Chen, Y. Wang and T. Ma, *J. Mater. Chem. A*, 2020, **8**, 4735-4739.
26. J.-T. Ren, L. Chen, H.-Y. Wang and Z.-Y. Yuan, *ACS Appl. Mater. Interfaces*, 2021, **13**, 12106-12117.
27. J.-T. Ren, L. Chen, Y. Liu and Z.-Y. Yuan, *J. Mater. Chem. A*, 2021, **9**, 11370-11380.
28. M.-C. Kim, H. Nam, J. Choi, H. S. Kim, H. W. Lee, D. Kim, J. Kong, S. S. Han, S. Y. Lee and H. S. Park, *ACS Catal.*, 2020, **10**, 10577-10584.
29. A. Liu, X. Liang, Q. Yang, X. Ren, M. Gao, Y. Yang and T. Ma, *ChemElectroChem*, 2020, **7**, 4900-4905.
30. H. Huang, F. Li, Q. Xue, Y. Zhang, S. Yin and Y. Chen, *Small*, 2019, **15**, 1903500.
31. J. Yu, X. Ren, J. Lu, H. Bai, X. Wang, J. Hu and H. Huang, *J. Alloys Compd.*, 2022, **902**, 163862.
32. L. Qiao, G. Duan, S. Zhang, Y. Ren, Y. Sun, Y. Tang, P. Wan, R. Pang, Y. Chen and A. G. Russell, *J. Cleaner Prod.*, 2020, **250**, 119525.
33. M. I. Ahmed, L. J. Arachchige, Z. Su, D. B. Hibbert, C. Sun and C. Zhao, *ACS Catal.*, 2022, **12**, 1443-1451.
34. J. Wang, Z. Jiang, G. Peng, E. Hoenig, G. Yan, M. Wang, Y. Liu, X. Du and C. Liu, *Adv. Sci.*, 2022, **9**, 2104857.
35. P. Hohenberg and W. Kohn, *Phys. Rev.*, 1964, **136**, B864.
36. W. Kohn and L. J. Sham, *Phys. Rev.*, 1965, **140**, A1133.
37. G. Kresse and J. Furthmüller, *Phys. Rev. B*, 1996, **54**, 11169.
38. P. E. Blöchl, *Physical Rev. B*, 1994, **50**, 17953.
39. J. P. Perdew, K. Burke and M. Ernzerhof, *Phys. Rev. Lett.*, 1996, **77**, 3865.
40. H. J. Monkhorst and J. D. Pack, *Phys. Rev. B*, 1976, **13**, 5188.
41. C. Zhao, S. Zhang, M. Han, X. Zhang, Y. Liu, W. Li, C. Chen, G. Wang, H. Zhang and H. Zhao, *ACS Energy Lett.*, 2019, **4**, 377-383.
42. Q. Zhang, F. Luo, Y. Ling, S. Xiao, M. Li, K. Qu, Y. Wang, J. Xu, W. Cai and Z. Yang, *J. Mater. Chem. A*, 2020, **8**, 8430-8439.